Numerical Study on Dynamical Downscaling for Regional Climate Projection

– Application to Asian Regions and Development of a Regional NICAM –

April 2014

Masayuki HARA

Numerical Study on Dynamical Downscaling for Regional Climate Projection

– Application to Asian Regions and Development of a Regional NICAM –

A Dissertation Submitted to
the Graduate School of Life and Environmental Sciences,
the University of Tsukuba
in Partial Fulfillment of the Requirements
for the Degree of Doctor of Philosophy in Science

Masayuki HARA

Abstract

In this paper, we have achieved a series of dynamical downscaling studies over the Asia region and development of a new regional climate model. First, we present the advantages of dynamical downscaling with three applications of a regional climate model (RCM). A RCM generally offers a better representation of atmosphere phenomena near the ground surface because of detailed topographic features, land cover, cumulus convection and local circulation than general circulation model (GCM). Next, we introduce a newly developed RCM to obtain more accurate near-future predictions.

Using this advantageous dynamical downscaling method, we have studied snow and an urban heat island of regional future climate change. A series of numerical experiments was conducted in order to investigate the impact of global warming on snow amounts in Japan during early winter. After confirming the accuracy of hindcast simulations for a high-snow-cover (HSC) year and a low-snow-cover (LSC) year, dynamical downscaling experiments were conducted in order to make future projections using the pseudo-global-warming method. The precipitation, snow depth, and surface air temperature of the hindcast simulations show good agreement with the AMeDAS station data. At the end of December, the decreasing ratios of snow water are more significant in areas with an altitude of less than 1,500 m. The increase in air temperature is one of the major factors influencing the decrease in snow water since the present mean air temperature in most of these areas is near 0 °C even in winter. On the other hand, the change in the mean areal precipitation due to global warming is less than 15 % in both years. The results indicate that the future snow change is strongly affected by detailed topographic features. Dynamical donwscaling, which can represent detailed topographic features, can produce improved snow projection over those of coarse grid GCMs.

During the past 100 years, the mean surface air temperature (SAT) increased about 3 °C in Tokyo, while the world mean SAT increased only 0.66 °C. The major reason of the difference in warming is the effect of the urban heat island (UHI), whose intensity also increased during the period and often the most during winter. This study investigates the change in

UHI intensity (UHII) of the Tokyo metropolitan area by the effects of global climate change. The present climate simulation is conducted using a high-resolution numerical climate model, the Weather Research and Forecasting (WRF) model, including an urban canopy sub-model. A future climate run is conducted using the pseudo-global-warming method, assuming the boundary conditions in the 2070s estimated by a GCM under the SRES A2 scenario. The simulation results indicated that UHII would be enhanced more than 20 % during the night due to the global climate change. SAT in the Tokyo metropolitan urban area increases more slowly during the daytime due to the larger heat capacity than in rural areas. Heat release from the buildings in the urban area is larger than that in rural areas at night, when the dispersion of the released heat tends to be restricted to the lower atmosphere because of weak turbulence. These processes are sensitive to cloud fraction and atmospheric stability in the lower atmosphere. The result shows that detailed land cover plays an important role in projecting future urban thermal environments. Dynamical downscaling of a GCM projection using RCM is necessary to obtain a detailed urban thermal environment because dynamical downscaling can capture the detailed land cover.

Next, we investigate precipitation over the Maritime Continent, comparing the precipitation simulated by a 20-km grid Meteorological Research Institute General Circulation Model (MRI-GCM) and the near-surface rain data of TRMM 2A25. The focus is particularly on the diurnal cycle and its phase distribution of precipitation. The features of the simulated precipitation mostly agree with observations made over islands and straits having horizontal scales smaller than 200 km. However, these are quite different around larger islands, such as Sumatra and Borneo, particularly in the phase of the diurnal cycle. The MRI-GCM indicates maximum precipitation in the early afternoon on these islands, while the observed precipitation has its maximum at night. In particular, over the inland areas of the larger islands, the simulated diurnal cycle has an almost reversed phase. The simulated precipitation is remarkably weaker than the observation around the western coast of Sumatra Island, where a large discrepancy is also found in the phase distribution along a line perpendicular to

the coast. A higher-resolution simulation using a non-hydrostatic model without convective parameterizations substantially improves the phase distribution over Borneo Island. The non-hydrostatic model simulates well the migration of the precipitation zone and the daily maximum at night in the inland areas. In contrast, the GCM fails to simulate the diurnal cycle over islands whose horizontal scale is larger than 200 km, although the 20-km grid spacing is small enough to reproduce the major aspects of the local circulations. The cause of the difference between the GCM and RCM is the cumulus convective parameterization, which may not adequately represent the coupling of convection and local circulations.

A new regional atmospheric model to target a certain limited area is developed for conducting realistic regional climate simulations based on the stretched horizontal grid version of a regional model based on the global cloud-resolving model, the nonhydrostatic icosahedral atmospheric model (NICAM). The simulation domain of the newly developed regional climate model (hereafter diamond NICAM) consists of one diamond (two triangles in an icosahedron), although the original NICAM global domain consists of ten diamonds (twenty triangles). Preliminary experiments with the diamond NICAM have been performed, and the results show almost the same climate as those of the global NICAM. Usage of the diamond NICAM can reduce the inconsistency in climate simulations between GCMs and RCMs.

keywords: *limited area atmospheric model, regional climate, dynamical downscaling, Asia, climatology*

Contents

List of Figures

List of Tables

Chapter 1

INTRODUCTION

1.1. General background

Climate change studies have achieved amazing developments after the publication of the First Assessment Report of Intergovernmental Panel for Climate Change (IPCC) in 1990 (Intergovernmental Panel on Climate Change 1990). Many researchers had performed and analyzed the simulations using general circulation models (hereafter, GCMs). Most simulations and/or projections using GCMs have been performed with coarse horizontal intervals as large as O(100km). In planning mitigation and adaptation for climate change, policymakers and/or researchers who are not majoring in climatology sometimes required climate data with less than 10-km resolution. The required resolution is less than 1-km in some cases.

In general, we have some ways to get high-resolution climate data. Downscaling methods can be categorized into dynamical downscaling or statistical downscaling (Mearns et al. 2003). Figure 1-1 shows various methods of downscaling climate data. Wilby et al. (2004) stated that there were three methods in statistical downscaling, i.e., weather typing, weather generator, and regression methods. The dynamical downscaling method is also categorized into three methods (Mearns et al. 2003; Warner 2010). The ideal and best way to obtain high-resolution climate data is a direct simulation by a super-high-resolution atmospheric GCM (AGCM). However, the super-high-resolution AGCM requires too high a computational cost to perform long-term simulations and/or projections (i.e., more than ten years) to analyze

climate change in the present circumstances. Instead of a super-high-resolution AGCM, we can use stretched grid AGCMs and regional climate models (RCMs). The computational cost of these models is lower than that of the super-high-resolution AGCM simulation.

Some downscaling methods have been developed to fill in gaps between GCM projection and social demands. In Chapter II and III, we performed dynamical downscaling simulations. In Chapter IV, we developed a new regional climate model to reduce uncertainty caused by the inconsistency of the physical process schemes and dynamical framework of GCMs and RCMs.

1.2. Dynamical downscaling of climate simulations and projections

As we mentioned in Chapter 1.1, simulations and/or projections for climate studies performed by atmosphere-ocean coupled GCMs (CGCMs) or Earth system models (ESMs) are still O(100km). Downscaling techniques are applied to CGCM or ESM simulation and/or projection because the super-high-resolution GCM simulation is rarely performed even on state-of-the-art supercomputers. Such a technique requires less than the super-high-resolution GCM simulation.

There are two techniques in downscaling. One is dynamical downscaling. Dynamical downscaling is a resolution enhancement method in which a higher-resolution RCM is nested in coarse GCM results. The other is statistical downscaling. Statistical downscaling is a method to enhance the resolution of future climate projections by using statistical relationships between present-day observations and simulations in the present-day climate. This method requires less computational cost than dynamical downscaling. The certainty of the method is not guaranteed, because the statistical relationship can be changed in the future climate.

Dynamical downscaling has some advantages compared to super-high-resolution GCM simulation and statistical downscaling. Specific examples of dynamical downscaling can be cited such as orographic precipitation caused by detailed orography, urban heat island

according to detailed land use and land cover, and explicit calculation of cumulus convection with a microphysics scheme. In this paper, we study the results of dynamical downscaling, namely, the advantage of regional climate model simulations and/or projections over coarse GCM results.

1.3. Regional climate studies using regional climate models

Future global climate studies grew up rapidly after the publication of the First Assessment Report (FAR) of the IPCC (Intergovernmental Panel on Climate Change 1990). Regional climate studies also started in earnest in the same period. In the end of the 1980s, dynamical downscaling of GCM future scenarios such as doubled CO_2 experiments was performed as a first attempt at National Center for Atmospheric Research (NCAR), U.S. In that attempt, Mesoscale Model version 4 (Anthes et al. 1986, MM4) was used as an RCM. Initial and lateral boundary conditions were obtained by NCAR Community Climate Model (CCM) simulation results. The resolution of the CCM is about 500 km, whereas the resolution of the MM4 was more than 50 km at that time (Dickinson et al. 1989; Giorgi and Bates 1989; Giorgi 1990, 1991; Giorgi and Mearns 1991; Anthes et al. 1986). The MM4 can resolve the topographic features of "continental scale" mountain ranges, which are larger than hundreds of kilometers, although the CCM cannot capture the detailed structure of the Rocky Mountains because of such a coarse horizontal resolution. The targets of dynamical downscaling were varied. Dickinson et al. (1989) performed simulations to obtain a highly resolved precipitation distribution to decide where to deposit a high-level nuclear repository. Giorgi and Bates (1989); Giorgi (1990, 1991); Giorgi and Mearns (1991) tried to simulate and analyze the precipitation and hydrological budget around the Rocky Mountains. After that, regional climate studies were carried out targeting North America, Europe, and Australia (Anthes 1990; Cohen 1990; McGregor 1997). After the first age of regional climate study, detailed regional climate information was strongly required from not only climatologist but also policymakers and non-climatological researchers. Recently, in the United States and

Canada, the North American Regional Climate Change Assessment Program (NARCCAP) (Mearns et al. 2009) are organized to project detailed climate using multi-GCM milti-RCM model ensemble method to estimate sources of uncertainty.

In the EU community, a series of large projects on downscaling and regional climate was initiated, such as PRUDENCE (2001-2004), ENSEMBLES (2005-2009), and CORDEX (2010-) in the 2000s. They regards that ensemble experiments is essential to estimate uncertainty of future climate (Rummukainen 2010). All their project performed not a small number of multi model ensemble experiments, although the horizontal resolution was relatively low. The United Kingdom recently has a project, United Kingdom Climate Projections (UKCP). The project published 11-member 25-km mesh RCM results, especially targeted on lightning, snow, and surface wind (Brown et al. 2009; Boorman et al. 2010; Brown et al. 2010).

In Japan, three groups, the Meteorological Research Institute/Japan Meteorological Agency (Kida et al. 1991; Sasaki et al. 1995) with RSM, the Central Research Institute of Electric Power Industry (Kato 1999) with RegCM, and the National Institute for Environmental Studies (Emori et al. 2001) with CSU-RAMS have begun to study the regional climate. Their main target was to simulate detailed precipitation feature in east Asian monsoon region, such as Baiu/Meiyu rainband. In the 2000s, the Meteorological Research Institute/Japan Meteorological Agency (Sasaki et al. 2008; Japan Meteorological Agency 2005, 2008, 2013) (NHRCM), the Japan Agency for Marine-Earth Science and Technology (Hara et al. 2008, 2010; Kawase et al. 2009) with WRF, and the University of Tsukuba (Kusaka et al. 2012; Takane et al. 2012) with WRF studied energetically.

The horizontal resolution is getting higher in recent years (Warner 2010; Hong and Kanamitsu 2014). Recently, a series of large projects by the Ministry of Education, Culture, Sport, Science and Technology (MEXT), i.e., Sustainable Coexistence of Human Nature and the Earth, Research Revolution 2002 (Kyosei project; 2002–2006), and the Innovative Program of Climate Change Projection for the 21st Century (Kakushin project; 2007–2011), was

completed, and now the Program for Risk Information on Climate Change (Sousei Project; 2012–) is in progress. The Ministry of Environment (MOE) supported a large project the Global Environment Research Fund (S-5-3; 2007–2012) to perform organized regional climate projections.

The main target of dynamical downscaling supported by the Kyosei and Kakushin Projects was heavy rainfall. Their regional climate model explicitly resolved cloud convection in very high horizontal resolution to reduce uncertainty caused by physical parameterization, such as cumulus convective parameterization. On the opposite side, the S-5-3 and Sousei project are targeted on multi-GCM and multi-RCM ensemble simulations/projections to reduce uncertainty caused by differences of GCMs and RCMs.

The Japan Meteorological Agency (JMA) also has a series of projects to perform regional climate projections. They periodically published reports called the "Global Warming Projection report" beginning in 1996. First, the reports contained the analysis of GCM simulation and/or projection results. The reports included regional climate projections since 2001 (Japan Meteorological Agency 2001, 2003, 2005, 2008, 2013). In the first report including regional climate projection (Japan Meteorological Agency 2001), researchers performed a 40-km horizontal grid regional climate simulation targeting only the winter climate. In 2005, the horizontal grid size was half that of the Japan Meteorological Agency (2001), and whole-year simulations were performed (Japan Meteorological Agency 2005). Their targets were climatological change of surface air temperature, precipitation, and snowfall. They also performed summertime urban thermal environment simulation using an urban climate model with a 4-km horizontal grid in the report. In the latest report (Japan Meteorological Agency 2013), regional climate simulations and projections with a 5-km horizontal grid were performed, and the results were comprehensively analyzed, although the future scenario and GCM are limited (SRES A1b and MRI-AGCM3.2). The report covered a widespread field, such as surface air temperature, summertime and wintertime precipitation, relative humidity, solar radiation, and atmospheric stability.

The JMA also annually published the "Heat Island Monitoring Report" begining in 2004 (Japan Meteorological Agency 2004, 2012). In the first report, (Japan Meteorological Agency 2004), they performed urban thermal environmental simulations targeting only summertime clear, calm days (23 cases). They also carried out a 1-km horizontal grid simulation to verify horizontal resolution dependency. Recently, they showed an analysis of regional climate simulations targeting a summertime heat wave in the Kanto district with a 2-km horizontal grid regional climate model (Japan Meteorological Agency 2012).

The framework of the dynamical downscaling in which an RCM is used for regional climate simulation with GCM simulation results is almost the same as that described in (Jones et al. 1995). In general, the results of dynamical downscaling are strongly affected by GCMs. This causes some potential problems. One of the major problems is caused by the inconsistency of physical process parameterization between GCMs and RCMs. The influence of the inconsistency cannot be reduced in general dynamical downscaling.

Kimura and Kitoh (2007) developed a novel framework to avoid the large GCM biases to perform a regional climate projection. The framework is called the pseudo-global-warming (PGW) method. In the PGW method, initial and lateral boundary conditions are given by the sum of 6-hourly reanalysis data and the components of climate change, which are the monthly averaged differences between the present-day and future climates projected by GCMs. These boundary conditions are expected to have a similar climatology to those of the future climate projected by the GCM, but the daily evolution is similar to that in the present-day years. The PGW method allows a comparison of the climate in the present-day years and that in the PGW years, which is similar to the present-day years in terms of the interannual variation but includes future climatology.

The PGW method is widely adopted for regional future climate projections, such as Mongolian precipitation Sato et al. (2007), wintertime precipitation in Japan (Hara et al. 2008; Kawase et al. 2012), Baiu (Kawase et al. 2008, 2009), and urban thermal environment (Hara et al. 2010; Kusaka et al. 2012; Adachi et al. 2012). Recently, the horizontal resolution

of regional climate simulations is smaller than several kilometers (Hara et al. 2008, 2010; Kawase et al. 2009; Kusaka et al. 2012; Takane et al. 2012).

1.4. Purpose of this study

In this study, we perform and analyze simulations and projections targeting the winter climate over Asian regions. The first object is present-day and future climate changes of the urban heat island and seasonal march of snow over Japan. We also analyze the diurnal cycle of convective activity over the Maritime Continent from the simulations performed using a 20-km grid atmospheric GCM (AGCM) and satellite data. RCM simulations are also performed to elucidate the mechanism of the diurnal cycle of convective activity.

Another object of this study is to develop a new regional climate model to reduce the uncertainty of climate simulations and/or projections. The uncertainty of climate simulations and/or projections has various causes, such as uncertainty in future socioeconomic scenarios and errors in numerical models. One of the major sources of uncertainty is the inconsistency of physical parameterization between GCMs and RCMs. The inconsistency can be ignored if we can perform a super-high-resolution GCM simulation. However, it is difficult to obtain the super-high-resolution simulation and/or projection for the near future. The inconsistency can be reduced if we use an RCM that has the same physical process parameterization and dynamical framework as a GCM.

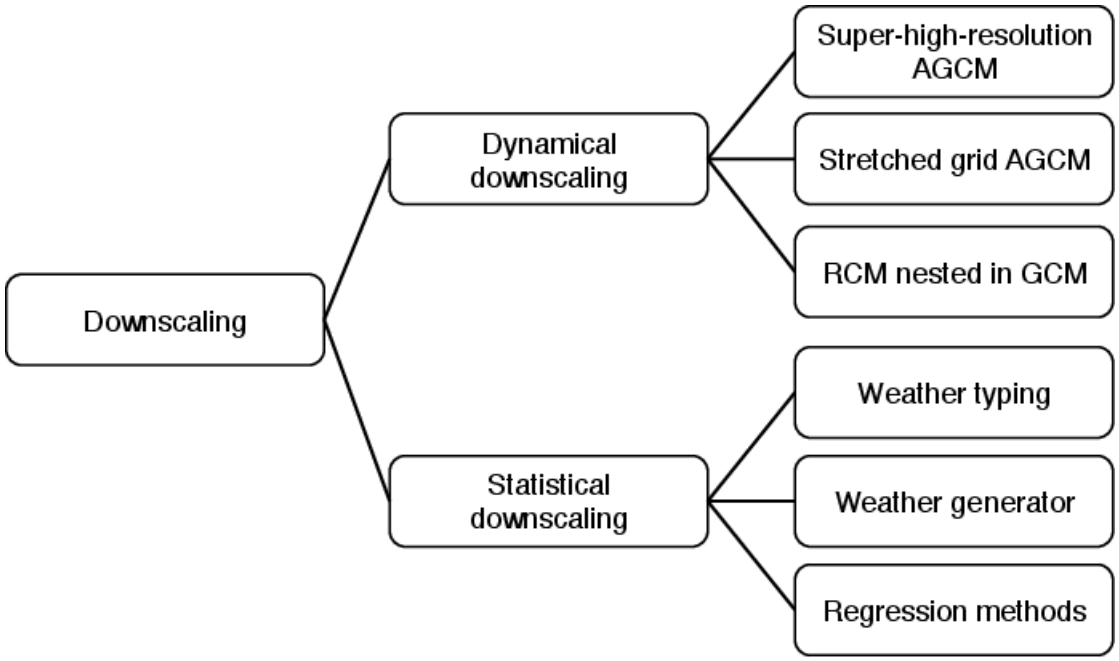

FIG. 1.1. Various methods in downscaling climate projections. (adapted from Mearns et al. 2003; Wilby et al. 2004)

Chapter 2

REGIONAL CLIMATE STUDIES OVER JAPAN

In this chapter, we show some examples of the application of the dynamical downscaling targeted on snow seasonal march and urban thermal environment over Japan in winter.

2.1. Regional climate simulation and projection of snow over Japan

Although a heavy snowfall often brings disaster, snow cover is one of the major water resources in Japan. Even during the winter, the monthly mean of the surface air temperature often exceeds 0 °C in large parts of the heavy snow areas along the Sea of Japan. Thus, snow cover may be seriously reduced in these areas as a result of global warming, which is caused by an increase in greenhouse gases.

Currently, most GCMs cannot reproduce local climates, which are directly related to orography (Intergovernmental Panel on Climate Change 2007). Other methods, such as dynamical downscaling (e.g. Kurihara et al. 2005; Japan Meteorological Agency 2008, 2013), statistical downscaling (e.g. Yokoyama and Inoue 2007), and direct simulation by high-resolution GCM (e.g. Hosaka et al. 2005), have been employed to project small-scale climate conditions. Extremely high horizontal resolution, i.e., a grid interval of less than several kilometers, is required to reproduce snow cover because the snow cover depends strongly on the local climate and small-scale orography.

Because of the large interannual variability of snowfall in Japan, long-term dynamical downscaling or ensemble projections are necessary in order to determine the change in snow

cover due to global warming. Long-term integration with a several-kilometer grid is, however, quite difficult to obtain because of a lack of computational resources. In order not to concern such a large year-to-year variability with short period numerical experiments, we use the Pseudo-Global-Warming (PGW) method.

The Pseudo-Global-Warming (PGW) method (Kimura and Kitoh 2007; Sato et al. 2007) is a dynamical downscaling method that allows the projection of regional climate change using a regional climate model. In the PGW method, initial and lateral boundary conditions are given by the sum of 6-hourly reanalysis data and the components of climate change, which are the monthly averaged differences between the present and the future climate projected by a GCM. These boundary conditions are expected to have similar climatology to those of the future climate projected by the GCM, but the daily evolution is similar to that in the present years. The PGW method allows a comparison of the climate in the present year and that in a PGW year, which is similar to the control year in terms of the interannual variation but includes future climatology.

The objectives are investigating the impact of global warming on snow amount in Japan during early winter. We used the PGW method to directly compare future snow depth with the present one without regarding the interannual variability. Numerical simulations in this study are performed with five-kilometer grid interval to include the effects of small-scale orography.

2.1.1. Design of numerical experiments

Our focus is the early winter (December) in 2005 and 2006. The former was an extremely High-Snow-Cover (HSC) year, while the latter was a typical Low-Snow-Cover (LSC) year during the 22-year period from 1985 to 2006. To estimate the difference of the impact of the global warming on snow amount between the HSC and LSC cases, we chose the two extreme cases.

The numerical study included four experiments: two realistic runs (CTL-HSC and CTL-

LSC) and two PGW runs (PGW-HSC and PGW-LSC). The CTL runs were simple hindcast runs using 6-hourly NCEP/NCAR reanalysis (Kalnay et al. 1996) for the boundary conditions, including SST given by the skin temperature of the reanalysis. To estimate the amount of snow in the 2070s, we applied the PGW method to both cases. The boundary conditions of the PGW runs were obtained through a reanalysis modified by the global warming components of the 2070s for monthly averaged air temperature, horizontal wind, geopotential height, and SST. The relative humidity was assumed to be the same as that of the present climate because the estimated change in relative humidity was small (Intergovernmental Panel on Climate Change 2007). The global warming components were estimated as the monthly averaged difference between the 10-year average of the 21st Century projection from 2071 to 2080 and the 20th Century simulation from 1991 to 2000 by MIROC 3.2 CGCM (Nozawa et al. 2007). The 21st Century projection was performed for 2001 to 2100 based on an A2 scenario presented by the IPCC Special Report on Emissions Scenarios (SRES) (Intergovernmental Panel on Climate Change 2000). The global warming components indicate that the air temperature rises 3-4 °C in the troposphere, while the SST rises 2-3 °C around Japan in December. A comparison of the CTL and PGW runs allows the projection of the change in snow depth due to global climate changes.

All simulations were conducted by two-way nesting using the WRF ARW-core model V2.2 (Skamarock et al. 2004). The coarse domain is covered by 120 × 100 grids at a 20-km grid interval, while the fine one is covered by 373 × 333 grids at a 5-km grid interval. Both domains have 27 vertical layers. The nudging technique was not used for the internal grid points in the experiments. The WRF-Single-Moment 6-class microphysics scheme and Noah land-surface model were adopted in both domains. The microphysics scheme separately estimates three categories of precipitation: rain, snow, and graupel. In this study, "snow" is assumed to be the sum of the latter two categories. The Noah-land-surface model includes a simple one-layer snow model that can simulate snow accumulation, sublimation, and melting. The simulations started at 00Z 21 November in each case and integrated six months each.

We assumed the first 10 days to be a spin-up duration.

2.1.2. Simulation of snow water equivalent

The simulated results are discussed by focusing on the study areas shown in Fig. 2.1 The observed snow depths at the end of December in the HSC and LSC cases are shown in Fig. 2.2a and d, while the simulated snow depths in the CTL-HSC and CTL-LSC runs are shown in Fig. 2.2b and e, respectively.

In the HSC case, the stations showing snow depths above 100 cm are distributed mostly in the central mountain range on Honshu Island, and those showing snow depths above 50 cm are distributed along the mountainous area even in southern Honshu Island, i.e., the San-in and Hokuriku areas (Fig. 2.2a). The snow cover is widely extended in the lower regions along the coast of the Sea of Japan and the Western Tohoku and Hokkaido areas. The simulated distribution of snow depth in the CTL-HSC run (Fig. 2.2b) agrees well with the observation. The extent of the snow cover, as well as the areas with a snow depth of more than 100 cm, is quite similar to those of the observation.

In the LSC case, heavy snow cover in excess of 100 cm is difficult to find at the AMeDAS stations, as shown in Fig. 2.2d, although the difference in the extent of snow is insignificant between the HSC and LSC cases. As shown in Fig. 2.2e, the CTL-LSC run accurately simulates these characteristics. Therefore, the heavy snow cover in the CTL-LSC over the mountainous areas is much less than that in the CTL-HSC run, but the extent of snow is not much different from that in the CTL-HSC run.

Table 2.1 shows the mean areal monthly precipitation observed at AMeDAS stations and the simulated one in the CTL runs. The former is the mean of all stations, and the latter is the mean of the grid point nearest each station in the study area. In the Hokkaido and Western Tohoku areas, the difference in the observed precipitation is small, i.e., within about 10 %, between the HSC and LSC cases. In the Hokuriku and San-in areas, located in the southern part of the snowy areas, the observed precipitation in the HSC case is as much as

twice that of the LSC case.

The differences between the observed and simulated precipitation amounts are less than about 30 % in all areas. The difference in the observed precipitation between the HSC and LSC cases is small, i.e., within about 20 % in the Hokkaido and Tohoku areas, while the simulated precipitation in the LSC case is less than 60 % of that of the HSC case in the Hokuriku and San-in areas. The differences of the area mean of the simulated precipitation between the HSC and LSC cases are almost same as the ones of the observation. These facts indicate that the simulated precipitation agrees well with the observation.

Fig. 2.3 shows the monthly mean air temperature at screen height in the HSC and LSC cases; in the Fig. 2.3a and d show the observations, and b and e show the CTL runs. In the HSC case, the observed temperature is about 0 °C in the lower parts of the San-in and Hokuriku areas. In the LSC case, on the other hand, the observed temperature is 3-5 °C in these areas, i.e., about 4 °C higher than that in the HSC case.

2.1.3. Projections of snow water equivalent

The PGW runs indicate and a smaller extent of snow cover, as shown in Fig. 2.2c (PGW-HSC run) and f (PGW-LSC run). The snow cover nearly disappears along the coastal areas on Honshu Island in the PGW-HSC run, while the extent of snow cover is significantly reduced not only along the coastal areas but also in the mountainous areas of Honshu Island in the PGW-LSC run. The areas where the air temperature is lower than 0 °C are almost same as the areas where the snow depth is greater than 0.1 cm by Fig. 2.2.

Table 2.2 indicates the snow depth in the five study areas in the CTL and PGW runs. The mean snow depth is calculated same as Table 2.1. The snow depth of the PGW runs in the southern area (Niigata, Hokuriku, and San-in) decreases to less than a quarter of those of the CTL in the HSC and LSC cases. Even in the northern area (Hokkaido and Western Tohoku), the snow depth in the PGW runs decreases to about one-third of those in the HSC and LSC cases.

Table 2.3 shows the total snow water in the areas categorized by the elevation of the ground surface. The study area is divided into the northern and southern areas according to the sensitivity of global warming to the snow depth, shown in Table 2.2.

Snow water decreases most drastically at elevations under 500 m in both cases of both areas. In the northern area, more than 90 % of the total snow water is distributed in the area lower than 1,000 m in the CTL-HSC and CTL-LSC runs. In the HSC case, the decreasing ratio of more than 50 % is limited in the area lower than 500 m, while it appears even at 500 to 1,000 m in the LSC case.

In the southern area, on the other hand, the decreasing ratio of more than 50 % extends to the areas lower than 1,000 m in the HSC case, and it covers the entire area in the LSC case. Snow water disappears at elevations under 500 m in the LSC case. The total snow water of the PGW in all of Japan is 38 % and 52 % of the CTL in LSC and HSC cases, respectively.

The snow cover change may depend on the precipitation and air temperature. As shown in Table 2.1, the precipitation changes between the CTL runs, and the PGW runs are less than 10 % in both cases, which suggests that the prominent reduction in the snow cover is caused primarily by an increase in the air temperature. The similarity between the horizontal distributions of changes in snow depth (Fig. 2.2) and air temperature (Fig. 2.3) is evident. The surface air temperature affects both the snowmelt water and the ratios of snow and rain to precipitation. Fig. 2.4 shows the ratio of snowfall to total precipitation. Although the ratio exceeds 80 % in a wide area of Japan in the CTL-HSC run, it decreases to less than 50 % in most of the lower areas in the PGW-HSC run. Even in the mountains, the ratio of snowfall seldom exceeds 50 % on Honshu Island. The distribution of the ratio of snowfall is also quite similar to those of snow cover and air temperature. These results suggest a simple mechanism for the reduction of the snow cover. The surface air temperature increases because of global warming, and the chance of snowfall then decreases so that snow cover is prominently reduced, particularly at the lower elevations of Honshu Island. The results of

the dynamical downscaling may depend on the boundary condition given by GCMs and its scenarios.

Figs. 2.5 and 2.6 show accumulated snow water equivalent all over Japan. The decrease of snow water equivalent exceeds 50 % and 70 % in HSC and LSC, respectively. The decrease is much more remarkable in LSC.

Yokoyama and Inoue (2007) estimated future snow depth by statistical downscaling using the projections given by six coarse-grid GCMs. They reported that the vulnerability of snow depth to global warming is significant in most areas along the coast of the Sea of Japan on Honshu Island, and that the reduction in snow water is primarily affected by the temperature, although the amount of precipitation depends on the GCMs. They estimated that the total snowfall in Japan would decrease by about 56 % after 100 years. Their results basically agree with our downscaling, except in Hokkaido, where they estimated an insignificant change in snowfall.

Japan Meteorological Agency (2013) recently estimated current and future snow in Japan with a 5-km horizontal grid regional climate simulations and projections. The future climate is projected by nonhydrostatic regional climate model (NHRCM) (Sasaki et al. 2008) with MRI-AGCM3.2 projection under SRES A1b scenario. Target period is 2016–2035 and 2076–2095. Wintertime future projection with several kilometer horizontal grid over Japan is less. So, it is worth to compare with our results, although the scenario and the periods are different from our numerical experiments. They stated that duration of snow cover and snowfall would be shorter than current climate. The result is consistent with our results. They also concluded that accumulated snow and snowfall would increase in inland area of Hokkaido, although accumulated snow and snowfall would decrease in Honshu island in future. In our results, accumulated snow decreases in all over the Japan. The difference can be caused by difference of future scenario, especially, SST in adjacent ocean to Hokkaido island Sasaki et al. (2012) explained the reason why the snowfall increases in future projection by the NHRCM.

We investigated the impact of global warming on snow depth in Japan during the winter of HSC and LSC using the PGW method. The CTL runs show good agreement with the observed precipitation in the HSC and LSC cases. The snow depth in the 2070s estimated by the PGW runs is substantially smaller than the present snow depth simulated by the CTL runs. In most areas, the snow depth of the PGW is less than 40 % that of the CTL in both cases. In the LSC case, the total snow water of the PGW is less than 38 % that of the CTL in all of Japan. In the HSC case, on the other hand, the total snow water of the PGW is 52 % that of the CTL since more than half of the snow water remains in mountainous areas at elevations in excess of 500 m. Reductions in snow depth are more prominent in the areas at elevations lower than 500 m in both the HSC and LSC cases. It is especially notable that the areas along the Sea of Japan on Honshu Island experience a reduction of three-quarters of the present depth.

These results depend on the GCM, which gives the boundary conditions of the RCM. In particular, the temperature change of the GCM will be quite sensitive to the change in snow depth and area. The decrease of the snow cover can be overestimated in our experiments, because, MIROC, the GCM adopted in this study, tends to give a slightly greater temperature change among the GCMs of the phase 3 of the Coupled Model Intercomparison Project (CMIP3). The projection of the snow cover is limited to December. The role of air temperature in the snow cover may change during the season of snowmelt water. For a detailed discussion of the change in snow cover through winter season, longer-term simulations are needed.

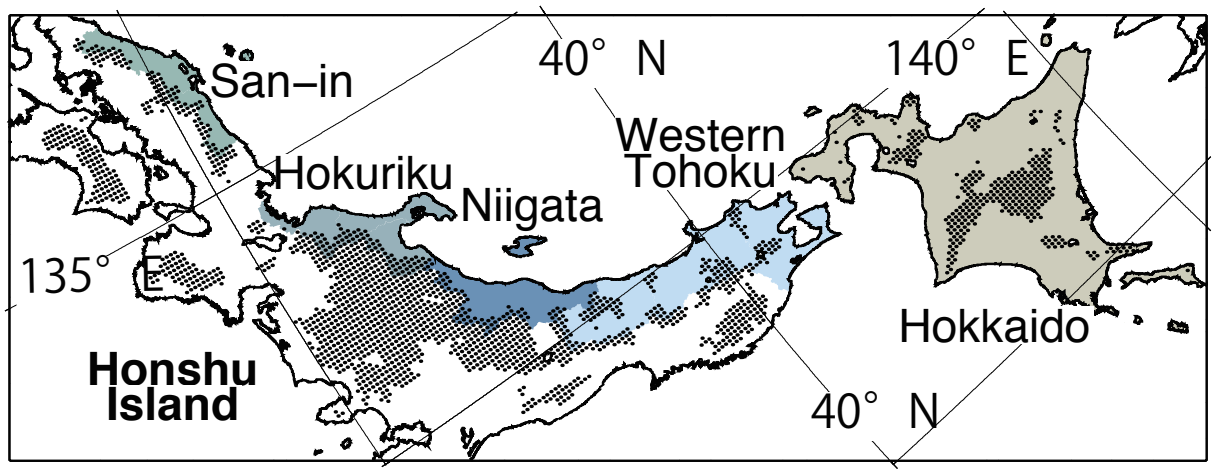

Fig. 2.1. Study areas and topographic altitude. Shaded areas indicate grid points located at elevations in exceeding of 500 m.

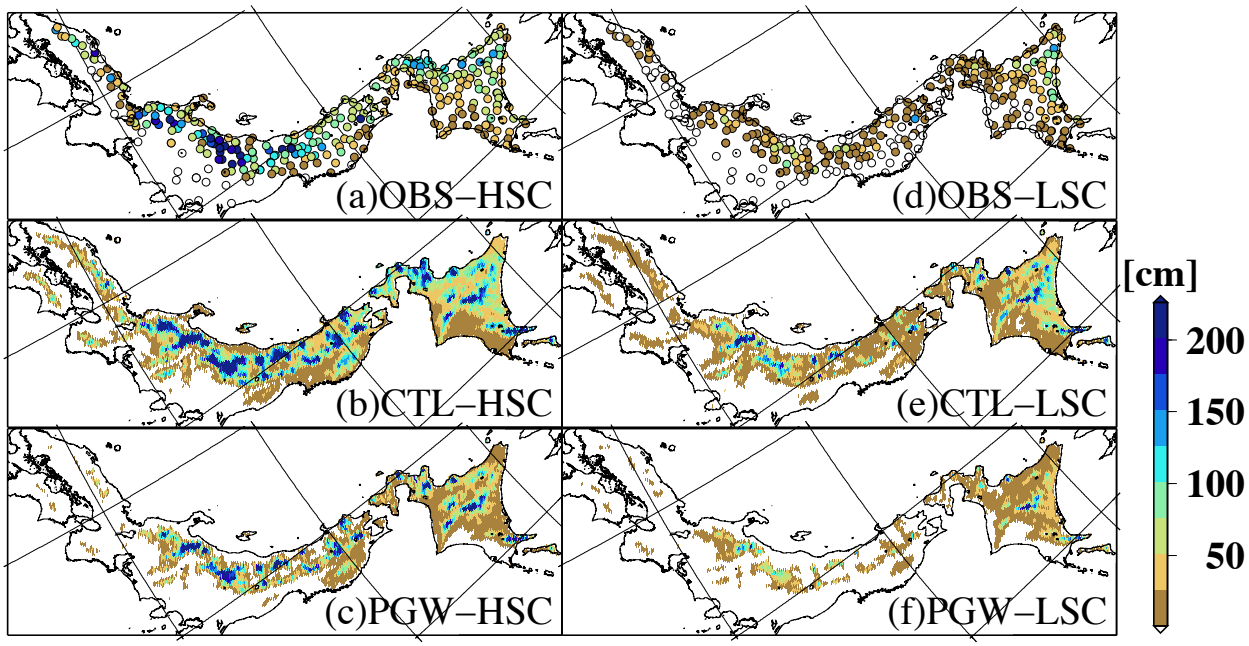

Fig. 2.2. Distribution of snow depth on 31 Dec, 2005 (HSC: a, c, e) and 2006 (LSC: b, d, f). Panels (a) and (b) indicate AMeDAS station data, (c) and (d), those of the CTL run, and (e) and (f), those of the PGW run.

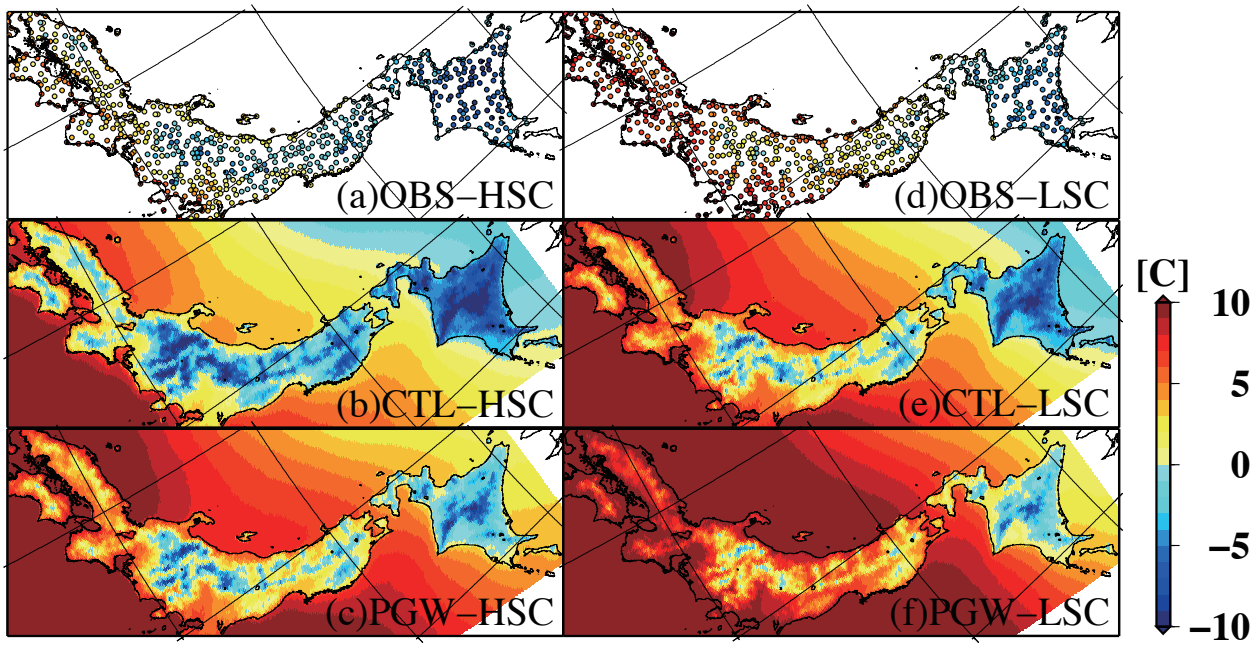

FIG. 2.3. Same as Fig. 2.2 except for the monthly averages of air temperature at screen height in December.

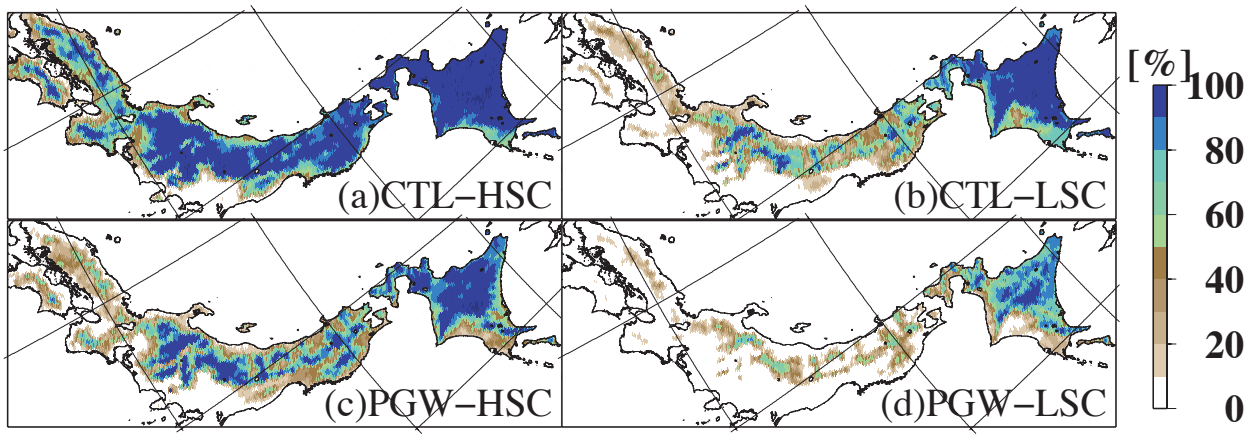

Fig. 2.4. Ratio of snowfall in the total precipitation in December estimated in (a) CTL-HSC, (b) CTL-LSC, (c) PGW-HSC, and (d) PGW-LSC.

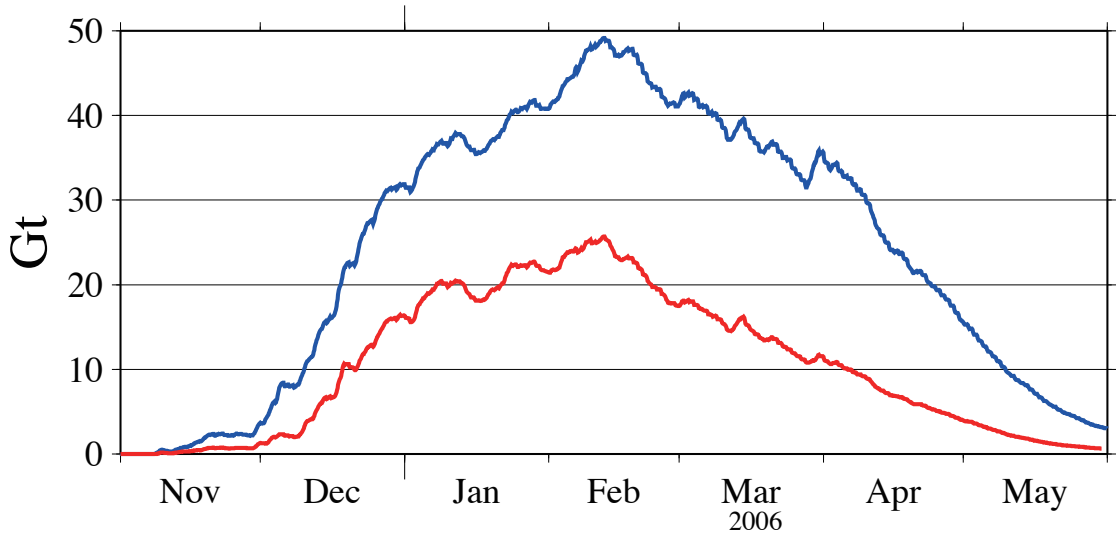

FIG. 2.5. Accumulated snow water equivalent all over Japan simulated by CTL-HSC (blue line) and PGW-HSC (red line).

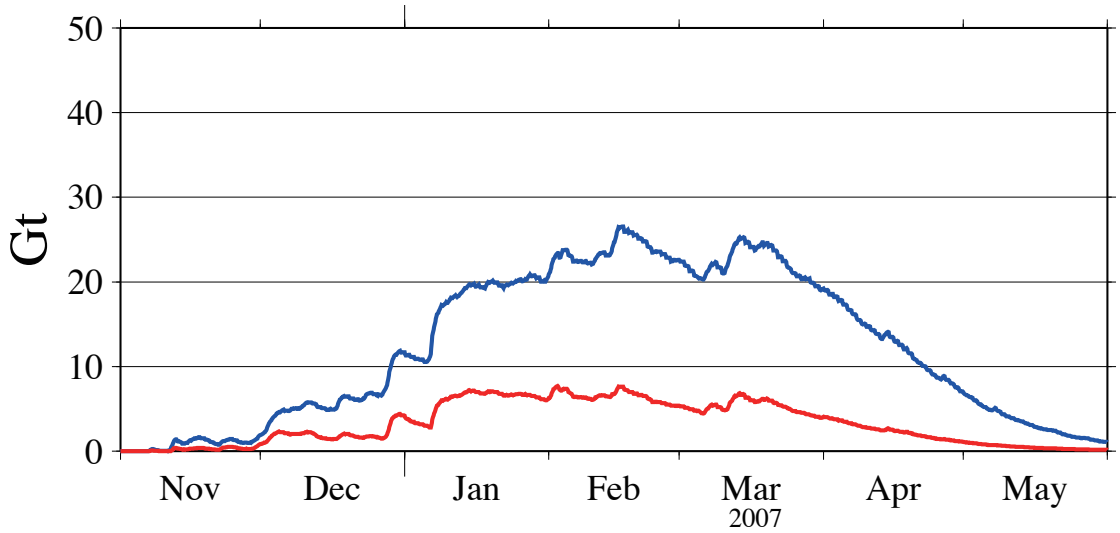

FIG. 2.6. Same as 2.5 but for CTL-LSC (blue line) and PGW-LSC (red line).

(mm)	Hokkaido	Western Tohoku	Niigata	Hokuriku	San-in
OBS-HSC	89.0	201.7	467.7	386.2	233.9
CTL-HSC	109.0	257.1	319.1	308.0	292.8
PGW-HSC	112.9	283.5	315.2	287.6	313.6
OBS-LSC	77.4	224.3	374.3	194.4	114.2
CTL-LSC	83.0	217.0	255.6	183.5	147.2
PGW-LSC	85.8	208.5	240.0	164.4	117.3

Table 2.1. Mean precipitation (mm) observed at AMeDAS stations (OBS-HSC and OBS-LSC) and those of the CTL and PGW runs in the study areas. The simulated precipitation represents the averages of the grid points nearest the stations.

	Hokkaido	Western Tohoku	Niigata	Hokuriku	San-in
CTL-HSC (cm)	40.7	50.7	49.1	80.1	23.7
PGW-HSC (cm)	14.8	14.8	10.8	5.7	2.7
PGW/CTL (%)	36.5	29.2	22.1	7.2	11.4
CTL-LSC (cm)	20.3	10.5	14.4	11.0	5.1
PGW-LSC (cm)	7.0	3.0	0.1	1.9	0.4
PGW/CTL (%)	34.4	29.0	0.5	17.7	7.7

Table 2.2. Mean estimated snow depth (cm) of the CTL and the PGW at the grid points nearest the AMeDAS stations. PGW/CTL indicates the ratio of mean snow depths of the PGW and the CTL.

(a) Northern part

(km)	0–0.5	0.5–1	1–1.5	1.5–	total
CTL-HSC (Gt)	8.2	5.9	1.3	0.09	15.5
PGW-HSC (Gt)	3.5	4.6	1.2	0.09	9.4
Decr. ratio (%)	57.3	22.0	7.7	0.00	39.4
CTL-LSC (Gt)	3.6	3.0	0.80	0.06	7.5
PGW-LSC (Gt)	1.1	1.4	0.54	0.06	3.1
Decr. ratio (%)	69.4	53.5	32.5	0.00	58.7

(b) Southern part

(km)	0–0.5	0.5–1	1–1.5	1.5–	total
CTL-HSC (Gt)	1.8	4.1	2.1	1.3	9.5
PGW-HSC (Gt)	0.20	1.8	1.6	1.0	4.6
Decr. ratio (%)	88.9	56.1	23.8	23.1	51.6
CTL-LSC (Gt)	0.24	0.78	0.71	0.55	2.3
PGW-LSC (Gt)	0.00	0.25	0.33	0.22	0.81
Decr. ratio (%)	100.0	67.9	53.5	60.0	64.8

Table 2.3. Total snow water (Gt) and the ratio of decreasing snow water in the PGW run and the total snow water in the CTL run of (a) northern area (Hokkaido and Western Tohoku) and (b) southern area (Niigata, Hokuriku, and Sanin) in the five levels categorized by the orographic elevation.

2.2. Regional climate of urban heat island over Tokyo metropolitan area in winter

Surface air temperature increase in metropolitan areas is one of major recent issues in urban area. The increase affects not only human health such as heat stroke, but also increasing infectious disease due to spreading out virus vectors habitat and increase of industry and house energy consumption. The temperature increase is mostly caused by global climate change and urban heat island (hereafter UHI) by urbanization. The population in Tokyo metropolitan area is over 30 millions and the Tokyo metropolitan area is one of the biggest megacities in the world. The temperature increase due to urbanization seems comparable to the global climate change in the major megacities. It is important to project how the urbanization and the global climate change affect to the future change of urban thermal environment to plan the adaptation and mitigation policy.

Seventeen stations in Japan have observed surface air temperature continuously since 1900. Temperature increase averaged all the stations from 1900 to 1999 is 1.1 °C. The temperature increase depends on urbanization. Increase in 3.3 °C at Tokyo station observed, and 2.0 °C increase observed averaged in Sapporo, Nagoya, Osaka, and Fukuoka. These increase are higher than that of 17 stations. This results implies that the urbanization is not negligible to estimate the future temperature change in the urban area in Japan.

Urban heat island intensity (hereafter UHII) is usually defined as the difference of surface air temperature between urban area and adjacent rural area. UHII from midnight to morning is relatively larger than that from noon to evening. The diurnal cycle of UHII is forced by larger anthropogenic heat, relatively smaller evapotranspiration because of small green cover area, and larger heat capacity of artificial buildings over urban area.

The UHII is generally large in early morning especially in winter. The temperature difference contrasted urban area with rural area, because radiative cooling develops surface inversion layer over rural area under clear sky in early morning.

Ichinose et al. (1999) created detailed maps of land use and anthropogenic heat over the Tokyo metropolitan area in summer and winter. They also calculated contribution of anthropogenic heat to surface air temperature change. The contributions is relatively larger in winter because the insolation in winter is smaller than the one in summer. The maximum anthropogenic heat exceeds 100 W m^{-2} in a part of the Tokyo metropolitan area. Usually, daytime insolation in winter is 500 - 600 W m^{-2} under clear sky around Japan. The anthropogenic heat reaches 10 % of insolation.

Many studies have been done since Kimura and Takahashi (1991) which performed numerical simulation including land surface process and anthropogenic heat in urban area targeted on the Tokyo metropolitan area. Recently, Kusaka and Kimura (2004) have employed an urban canopy model in the regional climate model. They stated that the regional climate model with an urban canopy model reproduced UHI better than the one with a slab urban model.

Future climate projections have been done by atmosphere-ocean coupled global climate model (CGCM) forced by greenhouse gas emission scenario. The horizontal resolution of the most of CGCM is larger than 100 km in CMIP5. The resolution is too coarse to represent the detailed land use and land cover information to estimate the thermal environment in a metropolitan area. Thus, we need to perform downscaling to estimate the thermal environment in detailed urban areas. Usually, we have two ways to downscale the CGCM information. One is dynamical down scaling, the other is statistical downscaling. Dynamical downscaling is a regional climate model simulation forced by CGCM and/or reanalysis data. Japan Meteorological Agency (JMA) performed 20-km grid regional climate simulation targeted on Japan. In Japan, S-5 project funded by Ministry of Environment and Research program on climate change adaptation, Innovative program of climate change projection for the 21st century, and Program for risk information on climate change by Ministry of Education, Culture, Sports, Science and Technology also leads many researches for dynamical and statistical downscaling studies.

Weather research and Forecasting (WRF) model (Skamarock et al. 2004) version 3 was developed in 2008 by National Center for Atmospheric Research and National Oceanic and Atmospheric Administration to simulate weather forecasting and to hindcast past meteorological phenomena. In the few years, many studies employ the WRF model to perform multi-year regional climate simulation.

There are few examples for climate regional projections targeted on urban heat islands. Urban climate simulations and/or projections require much computer resources, because the simulations and/or projections need both long-term integration and urban-resolved simulation with a few kilometer horizontal grids. RCM with a few kilometer horizontal grid intervals can simulate the urban heat islands because the structure of urban, suburban, and other land use types can be roughly represented (Kimura and Takahashi 1991; Kusaka and Kimura 2004; Adachi et al. 2012). Japan Meteorological Agency (2005) performed regional climate simulations and projections for typical several-days cases of summer clear days.

We performed one-month urban climate simulation and projection using a RCM. We focused on the surface air temperature in 2000's and 2070's Tokyo metropolitan area in December, because ecosystem is sensitive to change of wintertime minimum surface air temperature.

Target period in this study is December 2006. Observed monthly surface temperature around Tokyo metropolitan area is about 1 °C higher than climatology. The period is the third warmest December in 2000s at Nerima AMeDAS station. WRF ARW core V3.1.1 (Skamarock et al. 2004) model used for dynamical downscaling. The WRF model is finite difference method with full-compressible non-hydrostatic equation system. We used the WRF model as a RANS model in this study even though the WRF model can be used as not only RANS but also LES. Third-order Runge-Kutta scheme and time splitting is used in combination for temporal difference. Fifth-order upwind advection scheme and Second-order centered difference diffusion scheme in Arakawa-C grid system is used for spatial difference. Turbulent closure scheme is MYNN level 2.5 scheme (Nakanishi and Niino 2006; Mellor

and Yamada 1974). MYNN is based on Mellor-Yamada scheme (Mellor and Yamada 1974) but for more precise in calculating covariance terms of pressure and velocity deviations and turbulent length scale. The WRF model consists of fully-compressible non-hydrostatic equation system, equation for conservation of mass, energy, and water (vapor, liquid, and ice). Further information on the WRF model is reported by Kusaka (2009).

Six-hourly NCEP Global Tropospheric Analyses is used for initial and lateral boundary conditions in present climate simulation. The vertical layers are 45 layers and located from the surface up to 50 hPa, and vertical interval increases from 50 meter with height. We used one-way nested domains including coarser and finer ones (Fig. 2.7). The coarser domain and finer domain use 15 km and 3 km grid spacing, respectively. The time step for temporal integration is 15 seconds in the finer domain. Analysis domain is shown in Fig. 2.7. The shaded area in the Fig. 2.7 indicates urban area. The contour lines is orographic height with 500 meter interval. Fig. 2.8 shows domains for numerical experiments.

Noah LSM (Chen et al. 2011; Chen and Dudhia 2001) is used for land surface scheme with urban canopy model (Kusaka et al. 2001; Kusaka and Kimura 2004). The parameters used in the urban canopy model is shown in Table 2.4. The parameters didn't depend on urban density in our experiments. We used 100 meter mesh land use and land cover data composed by Ministry of Land, Infrastructure, Transport and Tourism in 1997. The data contains 11 land use categories. We treated the building area and arterial road as a urban area. The diurnal cycle of anthropogenic heat used in the simulation is given as Fig. 2.9. The daily mean of the anthropogenic heat is 19.2 W m^{-2}. WSM-6 microphysics scheme and RRTMG radiation scheme are adopted in the coarser and finer domains. Kain-Fritsch cumulus convective parameterization is used only in the coarser domain. It takes 40 hours to calculate one experiment (41 days) 36 cores of Intel Itanium 2 9040.

We performed a series of experiments as follows:

e• present climate simulation (CTL)

- present climate simulation without urban areas (CTLNU)

- future climate projection (PGW)
- future climate projection without urban areas (PGWNU)

Table 2.5 shows the design of each experiment. We assumed 2070's climate in PGW and PGWNU. The initial and lateral boundary conditions are NCEP FNL Global Tropospheric Analyses data in CTL and CTLNU. The simulation periods is from 09 LT 20 November 2006 to 09 LT 1 January 2007. The land use and the anthropogenic heat given in PGW is same as present climate. The areas which contain urban area is replaced by grassland in CTLNU and PGWNU. LAI in CTLNU and PGWNU is given same value as CTL.

We applied Pseudo Global Warming (PGW) method (Kimura and Kitoh, 2007; Sato et al., 2007; Sato 2010) for PGW and PGWNU. Monthly climate difference for PGW method is calculated from output data of MIROC T42 SRES A2 scenario projection (Nozawa et al., 2007). Present climate period is assumed from 1990 to 1999, future climate period is assumed from 2070 to 2079. The PGW method can reduce climate bias of GCM (Kawase et al., 2009). Hara et al. (2008) adopted the PGW method to wintertime climate projection over Japan.

2.2.1. Simulation of urban thermal environment

Fig. 2.10 shows monthly mean diurnal cycle of surface air temperature of observation and CTL at Nerima and Tsukuba AMeDAS (Automated Meteorological Data Acquisition System) station. The location of Nerima and Tsukuba is shown in lower panel of Fig. 2.7. The difference of the observation and simulation is less than 1 °C all through the day. Simulated surface air temperature slightly overestimated nighttime at Nerima and early morning at Tsukuba. The overestimation seems to be caused by the difference of spatial representativity between observation and RCM, simple treatment of urban land use category and the insufficient thickness of vertical layers.

Fig. 2.11 shows probability density functions of observed and simulated surface air tem-

perature at Nerima and Tsukuba. The PDF is well-simulated at Nerima. The PDF at Tsukuba also well simulated over 0 °C. Simulated surface air temperature shows unrealistic frequency maximum around 0 °C at Tsukuba. Because RCM doesn't have enough number of vertical levels to resolve ground inversion layer, simulatability of lower temperature may not be good. Treatments of frozen soil in the NOAH land surface scheme also affect to the bias in lower temperature conditions. Other AMeDAS observation sites (Tokyo and Ryugasaki) shows same manner as shown in Fig. 2.11 (not shown).

Fig. 2.12 shows monthly mean diurnal cycle of surface air temperature of CTL and CTLNU to evaluate the UHII in present climate. Difference of CTL and CTLNU in the daytime is relatively small at Nerima. The difference in the nighttime reaches 3 °C at Nerima. In Tsukuba, the difference is very small due to less urban area fraction. The decrease of surface air temperature at nighttime is small over urban area, because urban canopy reduces radiative cooling in nighttime (Kimura and Takahashi 1991; Kusaka and Kimura 2004). Fig. 2.13 shows UHII at 05 LT. Higher air temperature areas corresponds to the urban areas shown in Fig. 2.7.

2.2.2. Future projection of urban thermal environment

Fig. 2.14 shows air temperature and horizontal wind of synoptic scale climate change components at 850 hPa. The climate change components are calculated by MIROC T42 SRES A2 scenario. The temperature increase due to global warming over Tokyo metropolitan area is about 3 °C. Fig. 2.15 shows monthly mean diurnal cycle of surface air temperature of CTL and PGW. Thick long dashed and short dashed lines indicate temperature of climate change components at surface around Tokyo metropolitan area. The differences are almost constant all through the day at both stations.

We defined $UHII_{CTL}$ and $UHII_{PGW}$ as follows to evaluate UHII change due to global

warming.

$$UHII_{CTL} = T_{CTL} - T_{CTLNU} \tag{2.1}$$

$$UHII_{PGW} = T_{PGW} - T_{PGWNU} \tag{2.2}$$

Fig. 2.16 shows monthly mean diurnal cycle of $UHII_{PGW}$ and $UHII_{CTL}$ at Tsukuba and Nerima. $UHII$ is high from evening to early morning at Nerima. Difference of $UHII_{PGW}$ and $UHII_{CTL}$ is also large in nighttime, meanwhile the difference is small in daytime. The difference reaches 0.5 °C and the ratio, i.e., $(UHII_{PGW} - UHII_{CTL})/UHII_{CTL}$, is about 20 % in nighttime. $UHII_{PGW}$ and $UHII_{CTL}$ stay about zero at Tsukuba, because the area is away from urban area. Fig. 2.17 shows the monthly mean difference, $(UHII_{PGW} - UHII_{CTL})$, at 05 LT. The large difference areas correspond to the urban areas shown in Fig. 2.7.

We verified the present climate simulation (CTL) with AMeDAS observation data. The CTL is well-simulated for the monthly mean diurnal cycle of surface air temperature. Fig. 2.18 shows vertical profile of the air temperature of climate change components between 2070s and 1990s calculated by MIROC T42 SRES A2 scenario at 140 °E 35 °N. The climate change component increases with height. The atmosphere in lower troposphere can be much stable. Horizontal wind of climate change components shown in Fig. 2.14 shows anticyclonic deviation over Japan. The anticyclonic deviation corresponds to the change in stability (not shown). The change of stability in lower troposphere may cause the reduction of cloud fraction. The reduction may influence to surface radiative balance and urban thermal environment. Decrease of cloud fraction acts different role in nighttime and daytime. If cloud fraction decreases, the insolation in daytime can increase meanwhile the radiative cooling can be enforced near the surface.

Table 2.6 shows cloud fraction (all the day) and shortwave radiation (07-17 LT) of CTL and PGW. Cloud fraction decreases in lower and middle level and insolation increases by 3.6 W m^{-2} in PGW. Around urban areas, more insolation can be absorbed by buildings in

daytime, more stored heat can be released in nighttime.

Fig. 2.19 shows future climate projection by MIRCO T42 A2 scenario (upper panel) and WRF model (lower panel). It is difficult to recognize the regional feature of surface air temperature over Japan in the upper panel. The dynamical downscaling shows detailed spatial distribution of meteorological variables as shown in the lower panel. Thus dynamical downscaled data can be applied for many research fields such as architectural engineering, energy engineering, river engineering, agriculture, and biometeorology.

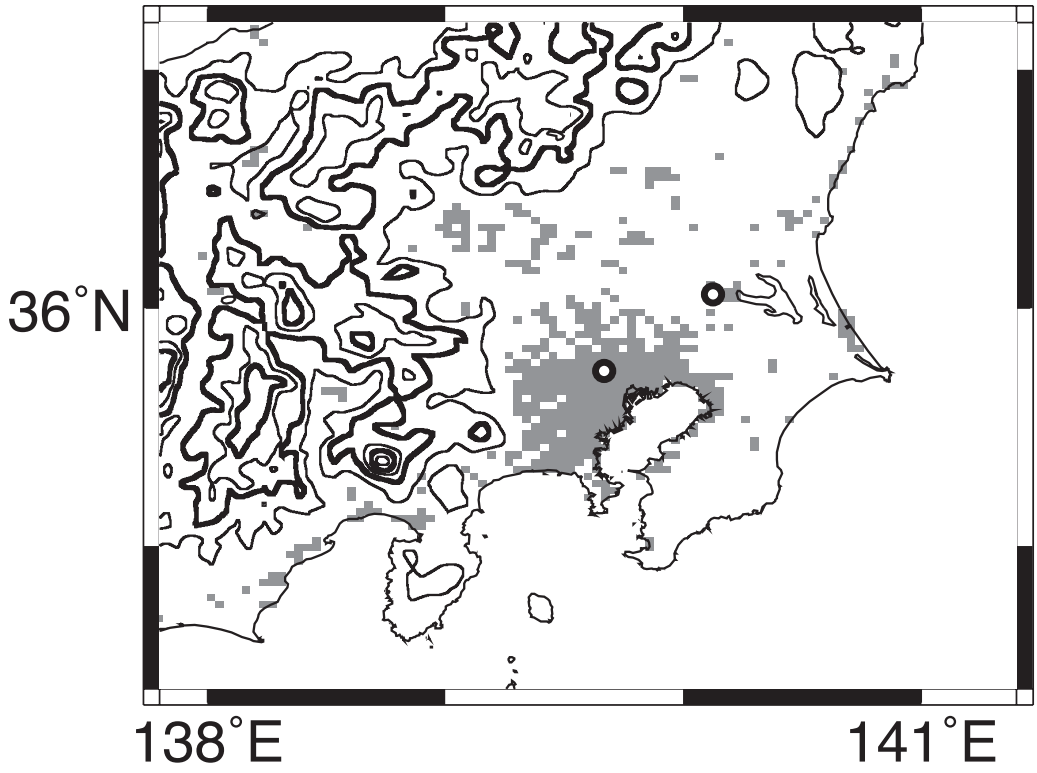

Fig. 2.7. Study area in this section. Gray shades indicate urban area in numerical simulation. Contour line shows topographic height. The interval is 500 m. Circles indicate Tsukuba (northern one) and Nerima (southern one) stations.

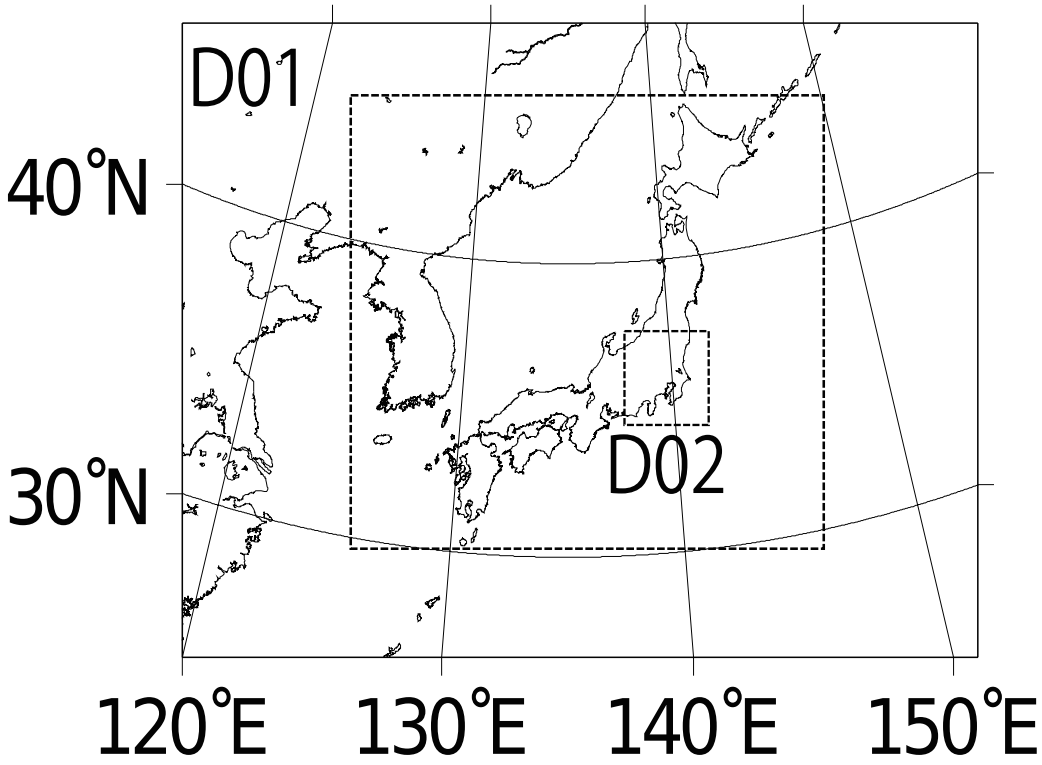

Fig. 2.8. Domains for numerical simulations.

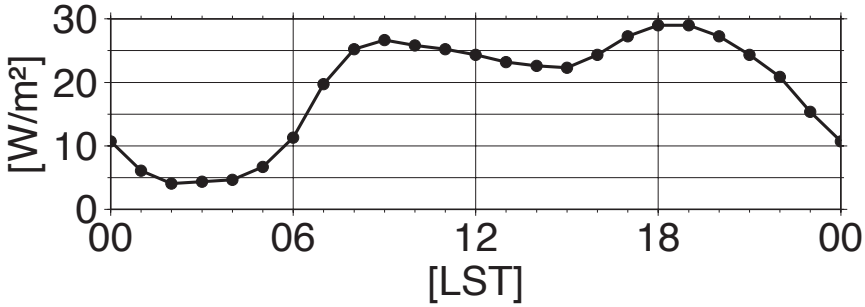

Fig. 2.9. Diurnal cycle of anthropogenic heat adopted in urban areas.

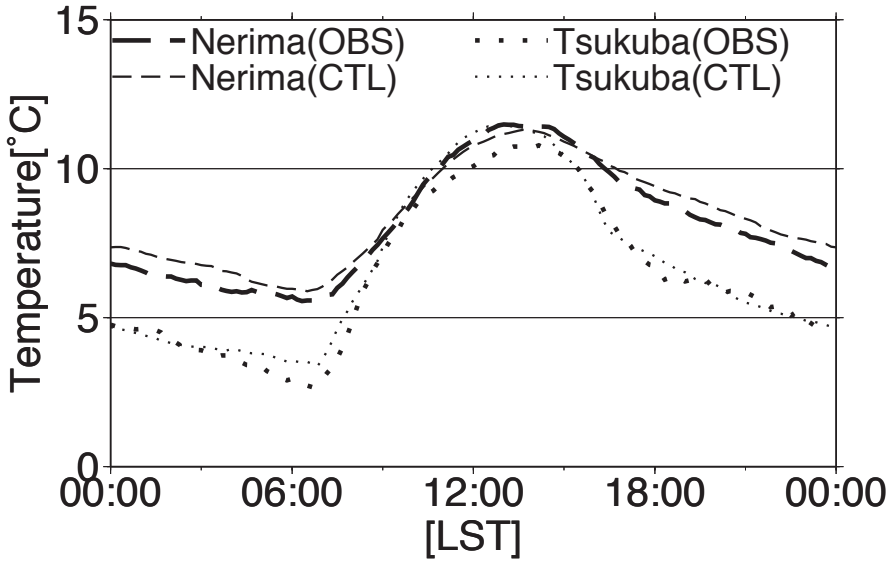

FIG. 2.10. Observed and simulated monthly averaged diurnal cycle of surface air temperature at screen height at Nerima (long dash and dash) and Tsukuba (short dash and dot).

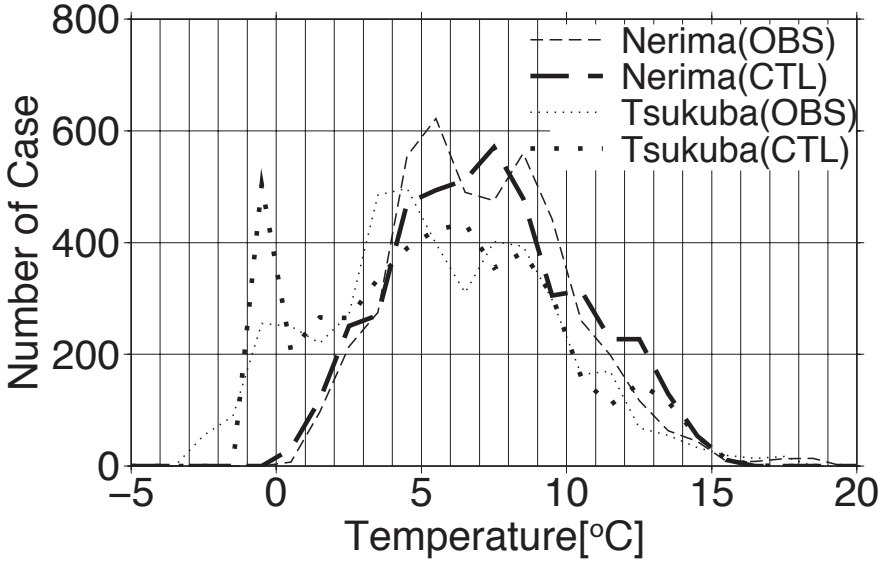

FIG. 2.11. Frequency distribution of observed and simulated 10-minute surface air temperature at screen height at Nerima (long dash and dash) and Tsukuba (short dash and dot).

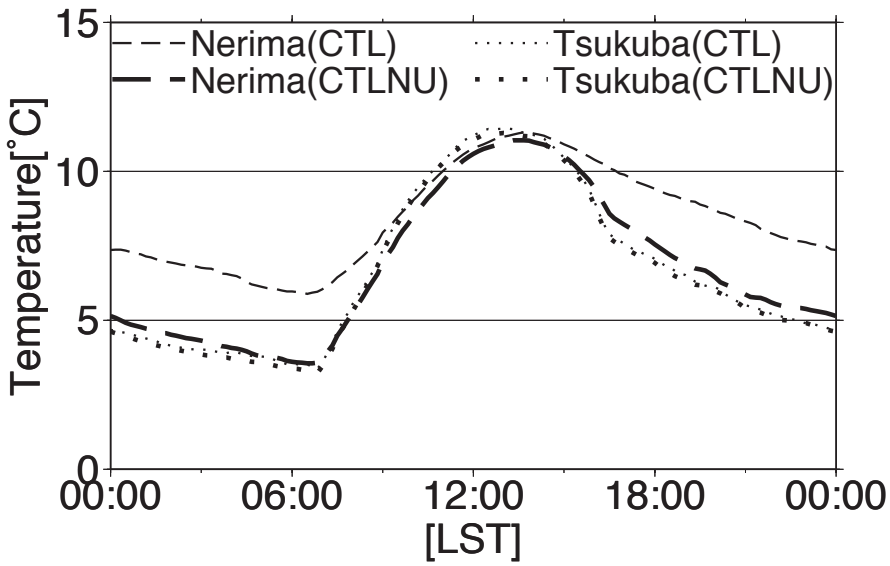

FIG. 2.12. Simulated monthly averaged diurnal cycle of surface air temperature at screen height at Nerima (long dash and dash) and Tsukuba (short dash and dot).

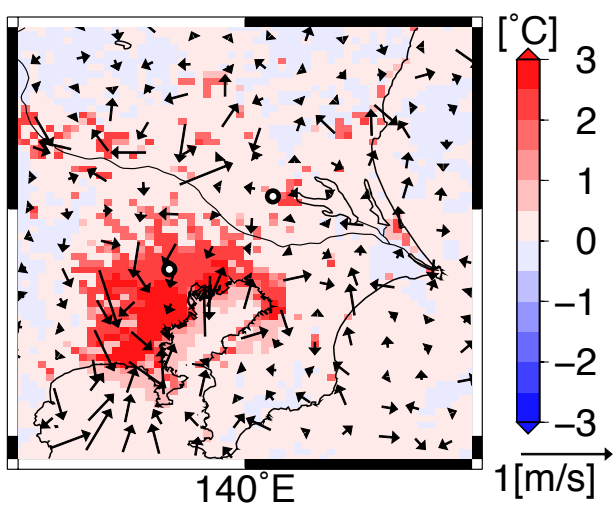

FIG. 2.13. Difference of monthly averaged surface air temperature and wind at 05 LT simulated by CTL and CTLNU.

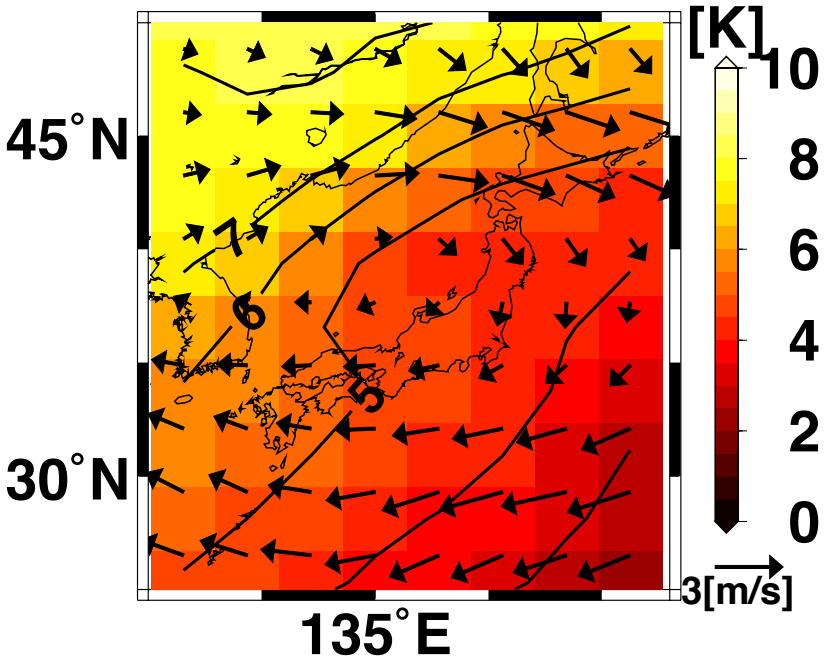

FIG. 2.14. Pseudo global warming component used in PGW and PGWNU experiments. Color shows air temperature at 850 hPa. Arrows show wind at 850 hPa.

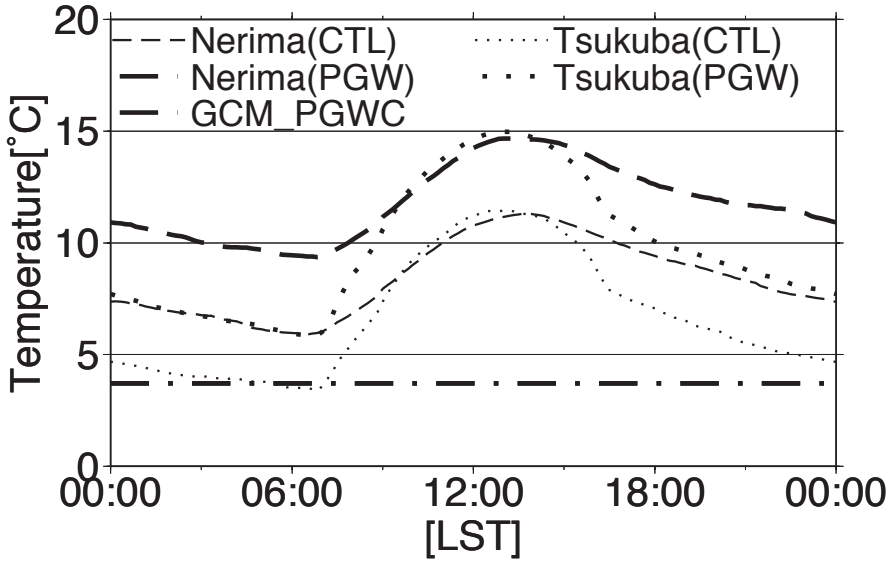

FIG. 2.15. Simulated monthly averaged diurnal cycle of surface air temperature at screen height at Nerima (long dash and dash) and Tsukuba (short dash and dot) by CTL and PGW. Dash and dot lines indicate PGW components of surface air temperature calculated by MIROC 3.2 medres A2 scenario.

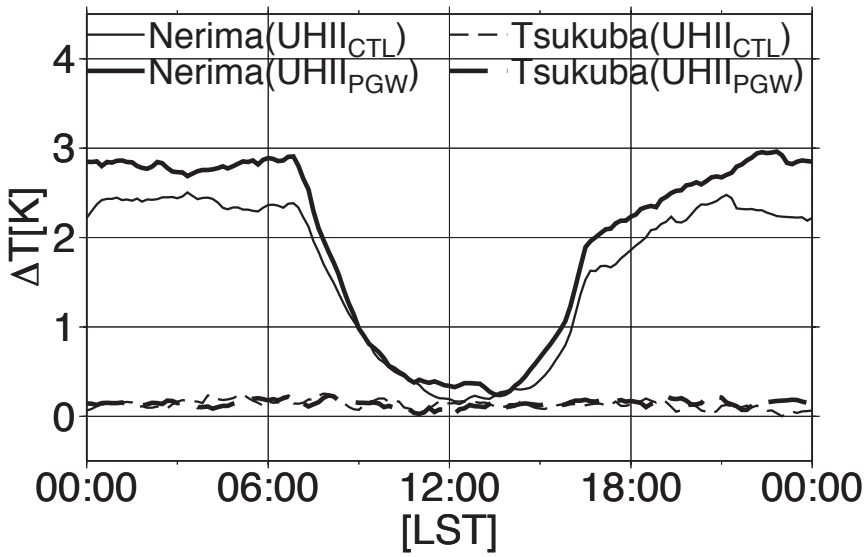

FIG. 2.16. Monthly averaged diurnal cycle of CTL and PGW at Nerima (thick and thin line) and Tsukuba (Thick and thin broken line).

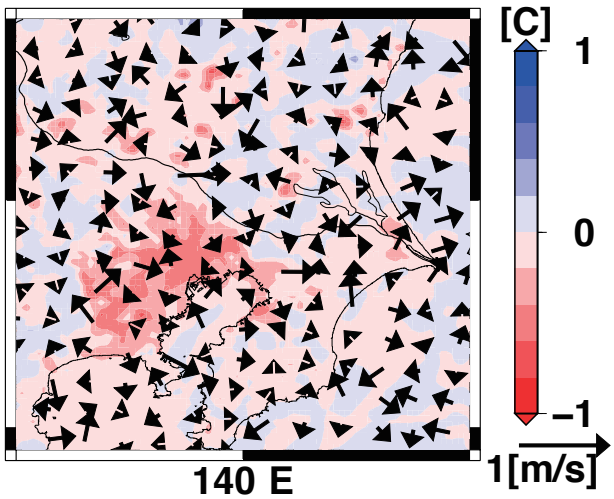

Fig. 2.17. Difference of monthly averaged UHII and wind at 15 LT simulated CTL and PGW.

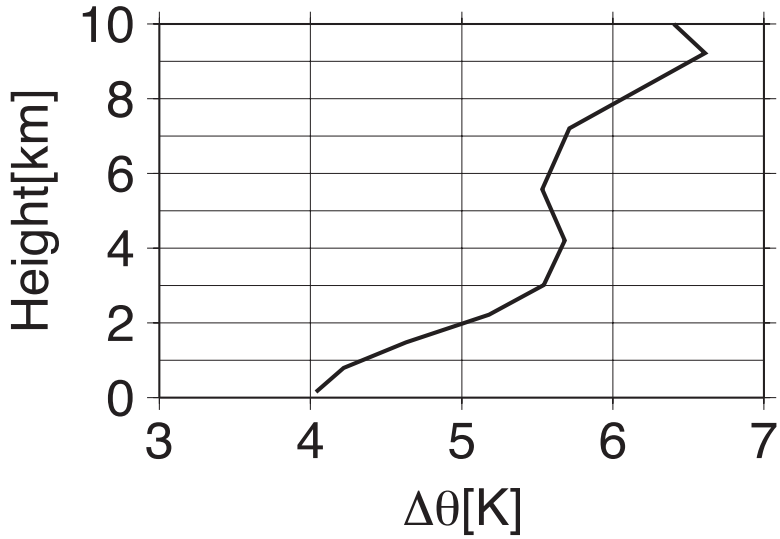

Fig. 2.18. Vertical profile of the difference of monthly averaged potential temperature in 2070s and 1990s at 140°E, 35 °N by MIROC 3.2 medres SRES A2 scenario.

(a)

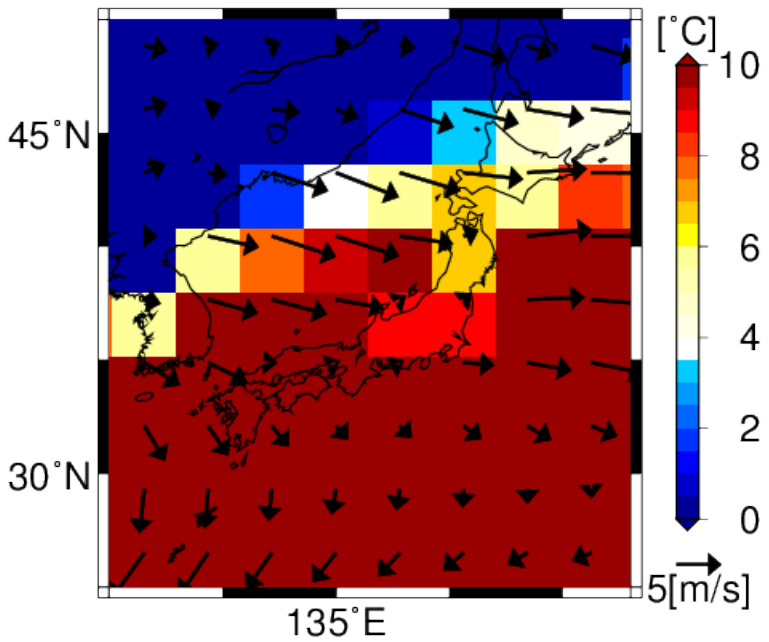

(b)

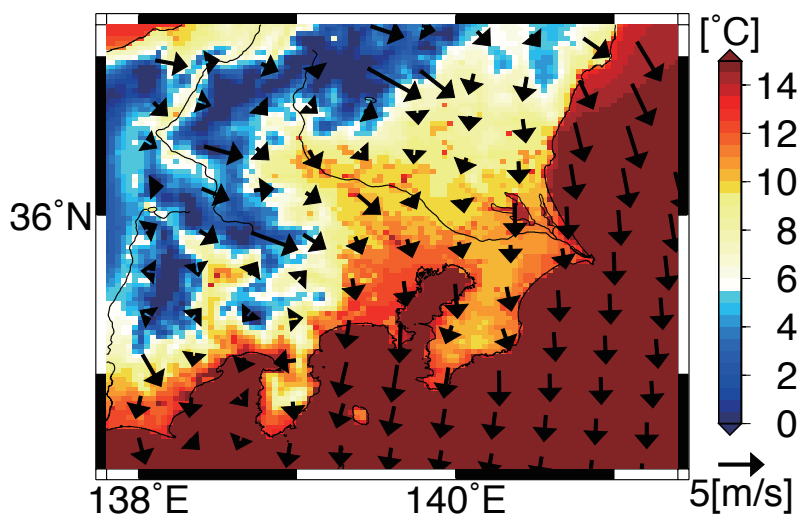

FIG. 2.19. 2070s' monthly mean surface air temperature at screen height (shade) and surface wind (arrows) projected by (a) MIROC 3.2 medres SRES A2 scenario and (b) WRF.

averaged building height (m)	9.0
building coverage (–)	0.5
green coverage ratio (–)	0.3
sky view factor (–)	0.56

TABLE 2.4. Parameters used in the urban canopy model.

Experiment name	PGW	Urban
CTL	no	urban area of 1997
CTLNU	no	replaced by grassland
PGW	applied (2070s)	urban area of 1997
PGWNU	applied (2070s)	replaced by grassland

TABLE 2.5. List of a series of experiments.

Experiment name	Downward shortwave radiation	low level cloud cover	mid level cloud cover	high level cloud cover
CTL	264.2	41	33	11
PGW	267.8	36	27	14
PGW-CTL	3.6	-5	-6	3

TABLE 2.6. Downword shortwave radiation (W m^{-2}) and cloud fractions (%) at three levels (low level is below 800 hPa, mid level is from 800 to 450 hPa, high level is over 450 hPa.) in each experiment.

Chapter 3

REGIONAL CLIMATE STUDY OVER THE MARITIME CONTINENTS

In this chapter, we show the verification and analysis on diurnal cycle of convective activity of 20 km-GCM simulation compared with TRMM satellite data. We also performed the simulation using a RCM to elucidate the mechanism of the diurnal cycle.

3.1. Diurnal cycle of convective activity analyzed in satellite data and 20 km-grid GCM

3.1.1. Comparison between TRMM 2A25 and MRI-GCM

The Maritime Continent is a well-known heavy-rainfall area. The intensive precipitation is not only a prominent local phenomenon there but also affects the planetary-scale atmospheric circulation (Neale and Slingo 2003). It is now widely accepted that most precipitation over the Maritime Continent is caused by a convective precipitation system in synchronization with a diurnal cycle. Earlier studies using Tropical Rainfall Measuring Mission (TRMM) data pointed out that the precipitation is primarily caused by mesoscale convective systems (MCSs) that are strongly forced by the diurnal cycle over the ocean on the western side of Sumatra Island (e.g. Nesbitt and Zipser 2003). In the past few years, several studies have analyzed the diurnal cycle of convective activity as simulated by GCMs (e.g. Neale and Slingo 2003; Collier 2004; Dai and Trenberth 2004; Dai 2006; Lee et al. 2007b,a). These GCMs

accurately simulate the large-scale distribution of precipitation, although the phase of the diurnal cycle tends to deviate significantly from the observation. The reasons for the phase discrepancy have been discussed and are presumed to be the extremely coarse grid spacing and incomplete cumulus parameterization schemes found in GCMs (Neale and Slingo 2003; Collier 2004). In particular, Dai (2006) studied the diurnal cycle of precipitation simulated by GCMs and stated that convections still tend to start earlier than the observation over land during the warm season, even in recent GCM simulations.

The diurnal cycle of convective activity simulated by GCMs largely depends on the horizontal resolution and cumulus convective parameterization of the GCM (Lee et al. 2007b,a). Lee et al. (2007b) carried out several tests of the sensitivity of a GCM to the horizontal resolution, using a range of mesh sizes from 0.5 to 2 degrees and focusing on the diurnal cycle of precipitation in the North American continent. They stated that some features of the diurnal cycle of precipitation can be better modeled by adopting a higher resolution, but large errors still remain, even with the highest horizontal resolution. Lee et al. (2007a) conducted some experiments to examine the sensitivity of the parameters in the relaxed Arakawa-Schubert scheme to the diurnal cycle. They found that the diurnal cycle strongly depends on the parameters. In most of these studies, it is difficult to accurately reproduce the diurnal cycle in the GCMs because the cumulus convective parameterization is not designed to represent MCSs.

Mizuta et al. (2006) conducted a numerical simulation using a GCM with a 20 km mesh called MRI-GCM TL959L60 that was developed by the Meteorological Research Institute, Japan Meteorological Agency (hereafter, MRI-GCM). The simulation yielded a significantly improved representation of precipitation including specific phenomena such as Baiu (Yasunaga et al. 2006; Kusunoki et al. 2006), the Asian monsoon (Yatagai et al. 2005; Mizuta et al. 2006), and tropical cyclones (Oouchi et al. 2006). Mizuta et al. (2006) also indicated that the model performance (e.g., the global distribution of precipitation and surface temperature) was drastically improved by the MRI-GCM, which can simulate local wind

circulation.

Arakawa and Kitoh (2005) investigated the diurnal cycle of the precipitation over a few islands around the Maritime Continent using the MRI-GCM. They reported that the MRI-GCM has the ability to reproduce thermally induced local circulation and that the phase of diurnal cycle of precipitation is also simulated around Java Island in Indonesia in good agreement with the TRMM observation. Although they investigated the phase of the precipitation, they did not determine the accuracy of the amount of precipitation. They stated that the accuracy of simulated local circulations was improved because of the finer grid spacing adopted by the MRI-GCM. However, the diurnal cycle of convective activity is not adequately simulated, especially over large islands such as Sumatra and Borneo, as seen in Fig. 1 of Arakawa and Kitoh (2005).

Thus, the diurnal cycle of convective activity over islands such as Sumatra and Borneo that have large precipitation amounts of more than 3000 mm/year is not simulated, even in the 20 km resolution GCM. This study investigates the features of precipitation simulated by the MRI-GCM in the Maritime Continent, especially around large islands, i.e., Sumatra and Borneo, in comparison with the precipitation observed by TRMM. The foci of this study are the following two points. The first is a detailed comparison of the spatial and temporal structures of the diurnal cycle on an "island scale", i.e., from tens to hundreds of kilometers. The second focus is the detection of the systematic phase error in the diurnal cycle of the simulated precipitation, which is closely related to the precipitation process.

3.1.2. Total amount of precipitation

Fig. 3.1 delineates the target domain of this study with the orographic height assumed in the simulation by the MRI-GCM. The MRI-GCM has 1920×960 horizontal grid points and 60 vertical layers. The horizontal grid spacing corresponds to almost 20 km. The bottom boundary conditions are the climatological monthly-mean SST and sea-ice concentration of the present climate. The duration of the simulation is 10 years, after a 5.5-year spin-up.

The details of the simulation have been summarized by (Mizuta et al. 2006). The simulation results are compared with TRMM 2A25 version 6 near-surface rain data (TRMM-NSR) provided by the National Aeronautics and Space Administration (NASA). To evaluate the climatological precipitation, we utilized eight-year-averaged precipitation data from 1998 to 2005. The hourly climatological precipitation is obtained in order to investigate the diurnal cycle of precipitation.

Fig. 3.2 plots the climatological mean annual precipitation over the Maritime Continent, where (a) indicates the ten-year-averaged precipitation obtained by the MRI-GCM, while (b) indicates the eight-year-averaged near-surface rain given by the TRMM-NSR. The simulated precipitation pattern agrees well with observations taken on small islands, such as Java Island and Sulawesi Island, whose widths are less than 200 km (R1 and R2 in Fig. 3.2). Areas of heavy precipitation (more than 3000 mm/year) were represented over the Makassar Strait and the Strait of Malacca (R5 and R6 in Fig. 3.2).

Although the positions of the local maxima of precipitation agreed fairly well with those of the observation, the amount of precipitation was seriously underestimated by nearly 2000 mm/year over the ocean to the west of Sumatra Island, while the simulated precipitation was significantly overestimated over the mountain range on the island (R3 in Fig. 3.2). A substantial difference in the precipitation distribution is also found over Borneo Island. The model simulates heavy precipitation over the mountains in the northern part of the island (R4 in Fig. 3.2), although heavy precipitation is actually observed over the southern part of the island.

Precipitation is considerably overestimated over a very wide area from 140°E to the eastern boundary of the figure and from the equator to 7 °N, as reported by (Mizuta et al. 2006). However, this discrepancy will not be discussed here because our focus is on precipitation in the Maritime Continent, especially around Sumatra and Borneo, as mentioned above.

3.1.3. Phase of diurnal cycle of precipitation

Fig. 3.3 and 3.4 portray the horizontal distribution of the local time of maximum precipitation in the diurnal cycle simulated by the MRI-GCM (Fig. 3.3a), that observed by the TRMM-NSR (Fig. 3.3b), and their difference (subtracting Fig. 3.3b from 3.3a) (Fig. 3.4). Fig. 3.3a indicates that the precipitation simulated by the MRI-GCM reaches a daily maximum in the late afternoon or the early evening (1600 to 1900LT) over most of the land surface, while the observed maximum in Fig. 3.3b appears only within limited areas over the land surface near the coasts during these periods. The time of maximum precipitation agreed well with most of the coastal areas and the straits. Particularly, the difference in the time of maximum precipitation is only a few hours on small islands, such as Java Island and Sulawesi Island, as well as over straits, such as Makassar Strait and the Strait of Malacca (R1, 2, 5, and 6 in Fig. 3.3a; white and red areas in Fig. 3.4). In the straits, the observed precipitation becomes the daily maximum from 0000LT to 0300LT.

In contrast, over the inland plains on large islands, such as Borneo Island and New Guinea Island, the time of maximum precipitation simulated by the MRI-GCM is almost 12 hours earlier than that of the observation (Fig. 3.4). The observation (Fig. 3.3b) reveals that the time of the maximum precipitation clearly depends on the distance from the coast of Borneo Island, and seems to migrate inland from the coast. However, the migration is unclear in the simulation, as seen in Fig. 3.3a. The simulated precipitation reaches its maximum in the late afternoon or the early evening (1600 to 1900LT) inland on these islands, while the observed precipitation reaches its maximum at night (2000 to 0400LT). The simulated maximum precipitation is more than six hours earlier than the observation over the ocean west of Sumatra Island and northwest of Borneo Island.

Fig. 3.5 indicates the climatological annual mean precipitation for each six-hour time slot in a day from the MRI-GCM and the TRMM-NSR. Periods 1, 2, 3, and 4 are defined as the respective time slots 0300 to 0800 LT, 0900 to 1400 LT, 1500 to 2000 LT, and 2100 to 0200 LT. In figures of both the simulation and the observation, a substantial amount of

precipitation is found in Periods 2 and 3 (0900 to 2000LT) on most of the small islands (Figs. 3.5b, 3.5c, 3.5f and 3.5g), while precipitation is quite weak in both the simulation and observation in Periods 4 and 1 (2100 to 0800LT) (Figs. 3.5a, 3.5d, 3.5e, and 3.5h).

A very small amount of precipitation is observed over the large islands, as seen in Period 2 (Fig. 3.5f), except for the areas along the coastline. In contrast, a large amount of precipitation is simulated over the islands in Period 2 (Fig. 3.5b). The amount of observed precipitation becomes large over mountain areas and the areas along the coastlines in Period 3 (Fig. 3.5g), while the simulated precipitation is already in the mature stage over large islands (Fig. 3.5c). In Period 4 (Figs. 3.5d and 3.5h), the simulated precipitation have already decreased, but the observed precipitation is still large over the islands, maintaining its intensity until Period 1 of the next day (Fig. 3.5e). These figures indicate that the simulated precipitation starts and ends earlier than that of the observation over large islands. The model simulated nighttime heavy precipitation (Period 1) observed over the ocean on the southwestern side of Sumatra Island quite poorly (e.g. Nesbitt and Zipser 2003; Mori et al. 2004; Hirose 2005).

The observed precipitation over Borneo Island is not very large in Period 2, but it increases to its maximum in Period 4 over the southern part of the island. The precipitation then gradually decreases but continues until morning (Period 1). However, the simulated precipitation is much larger than that observed by TRMM-NSR over the northern mountains in Period 2 (0900 to 1400LT) and reaches its maximum earlier, in Period 3.

Over the ocean to the southwest of Sumatra Island, the observed precipitation is still large in Period 1 (Fig. 3.5e), followed by that in Period 4, when the precipitation reaches its maximum (Fig. 3.5h). The simulated precipitation reaches its maximum at around midnight (Fig. 3.5d) but becomes quite weak in the early morning (Fig. 3.5a). The spatial distribution of the diurnal phase of the simulated precipitation changes discontinuously between the offshore and onshore areas on the western coastline of Sumatra Island, while the observed one changes continuously there.

Distance-time cross-sections of precipitation are presented in Figs. 3.6a and 3.6b, representing those of the MRI-GCM and the TRMM-NSR. The cross-sections are taken along Area A-A' around Sumatra Island (Fig. 3.1). The observed precipitation over the ocean near the coast intensifies at 2000 LT and remains until 0800 LT, extending westward (D1 in Fig. 3.6b), while the simulated precipitation area is small (Fig. 3.5d and 3.5a) compared to the observed precipitation, moving slowly toward the west from around midnight until about 0400 LT. As Mori et al. (2004) suggested, a convection system that is generated along the mountain range in the evening separates into two parts that propagate west and east at night. The convection system going west is quite active from midnight to early morning and results in heavy precipitation over the ocean up to about 200km off the coast. The simulated precipitation has some similarity in the time evolution of a convection system (D1 in Fig. 3.6a). However, the migration of the simulated precipitation area from the coastline to the west, which intensifies around 1200 LT over the coastline, has two local maxima, i.e., around 1200 LT on the coastline and 0000 LT (D01 in Fig. 3.6a). In fact, it briefly weakens around the coastline in the early evening, is then enhanced again around midnight, and finally disappears earlier than the observation. Although the observed precipitation area, which migrates to the inland area, moves continuously from the coastline to the inland area, the simulated precipitation area, which migrates from the coastline to the inland area, intensifies in the afternoon (1200 to 1500LT) and migrates inland around 1800LT. Another precipitation area appears separately from about 2000LT to the early morning (0600LT).

Fig. 3.7 is the same as Fig. 3.6 except for Area B-B' around Borneo Island. Precipitation is observed in a limited area over land along the coastline in the afternoon (1200 to 1500LT). This indicates that substantial precipitation begins near the mountain range along the coast. The precipitation area migrates toward the center of the island, arrives at the center of the island about 400 km away from the coastline at midnight (D3 in Fig. 3.7b). The convection then weakens around 0300 LT. In the late evening (2300 to 0200LT), the precipitation over the ocean near the coast begins to increase and propagates offshore. The amount of precipitation

reaches its maximum after midnight. Fig. 3.7a demonstrates that the MRI-GCM partially simulates the convection propagating offshore, although the intensity is underestimated and decreases much earlier than the observation. The propagation inland completely failed to be simulated (D2 in Fig. 3.7a). The simulated precipitation has an almost uniform diurnal cycle all over the island, with a maximum in the afternoon (1500LT), independently from the distance from the coast, although the observation clearly shows the inland migration.

3.2. Estimation of the diurnal cycle of convective activities simulated by regional climate model

Discrepancies in the diurnal cycle should strongly depend on the cumulus convection parameterization and grid spacing. We carried out a one-month simulation using a non-hydrostatic limited-area model, namely the Weather Research and Forecasting (WRF) model version 3.0.1.1 (Skamarock et al. 2004), with a two-way nested domain. Fig. 3.8 delineates the domain of the simulation. The outer domain (D01) has 176×152 grid points with 14km grid spacing; the inner domain (D02) has 536×416 grid points with 3.5 km grid spacing. Both domains have 31 vertical layers (surface to 50 hPa). The microphysics scheme that is used in this simulation is the WRF Single-Moment 6-class (WSM-6) scheme without cumulus parameterization. The National Oceanic and Atmospheric Administration (NOAA) Land-surface model and the Mellor-Yamada-Janjic (MYJ) TKE PBL scheme are also employed in the simulations. The experiments are carried out for one month, April 2004, using the initial and boundary conditions given by the NCEP Global Tropospheric Analyses. The simulation starts at 00Z 25 March 2004 and is integrated for 36 days. The first six days of the simulation are assumed to be spin-up. We analyzed the simulation output for the 30 days in April. Through the simulation period, no tropical cyclone is observed over Borneo Island, and the Madden Julian Oscillation (MJO) is inactive. Additionally, the diurnal cycle of convective activity is not disturbed by cyclones or synoptic scale disturbances in this

period. The surface ambient wind in the lower troposphere over Borneo Island is weak, almost dropping below 5 m/s in the NCEP Global Tropospheric Analyses (not shown).

Because the TRMM-NSR has too few samples to calculate the monthly diurnal cycle of precipitation, we used TRMM 3B42 version 6 (Huffman et al. 2007) to validate the one-month simulation of the WRF model. Fig. 3.9 indicates the one-month mean precipitation for each six-hour time slot in a day of (a) TRMM 3B42 version 6 (Huffman et al. 2007) and (b) the WRF simulation. In the WRF simulations (Figs. 3.9 b to f), the time slots are defined as 0300 to 0800 LT, 0900 to 1400 LT, 1500 to 2000 LT, and 2100 to 0200 LT. Because TRMM 3B42 is three-hourly data, the figures for TRMM 3B42 are the average of two three-hour data sets, i.e., 0500 LT and 0800 LT, 1100 LT and 1400 LT, 1700LT and 2000 LT, and 2300 LT and 0200 LT, which correspond to the time slots of the WRF simulations (Figs. 3.9 b to f).

The diurnal cycle of precipitation by TRMM 3B42 exhibits almost the same characteristics as the ten-year-averaged precipitation in Figs. 3.5 e to h. The observed precipitation over Borneo Island starts in early afternoon (1100 to 1400 LT) along the coastline and over the central mountains. The precipitation area extends and migrates into the inland area in 2300 to 0200 LT. The precipitation areas intensify and gather over the center of the island around midnight and survive until early morning (0500 to 0800 LT).

Most of the features of precipitation observed by TRMM are well simulated by the WRF model. The simulated precipitation distributes along the coastline in the afternoon (0900 to 1400 LT, 1500 to 2000 LT), and then the precipitation area migrates inland in the evening (2100 to 0200 LT). A heavy precipitation area arises in the center of the island in the early morning (0300 to 0800 LT).

Figs. 3.10 and 3.11 shows longitude-height cross section of monthly averaged mixing ratio of liquid and iceand longitudal and vertical wind at 16 LST and 00 LST at narrow region (Fig. 3.10) and wide region (Fig. 3.11). At 16 LST, cumulus convections are generated at the front of sea breases both of wide and narrow regions (Fig. upper panels of Figs. 3.10 and

3.11). Although convective activities decay at 00 LST in the narrow region (middle panel of Fig. 3.10), penetration of the sea breeze and convective activity survived in the wide region at 00 LST (middle panel of Fig. **??**).

Simulated surface wind also shows a clear diurnal cycle in thermally induced local circulations. Sea-breeze fronts form along the coastline over the island in the afternoon then penetrate into the inland areas in the evening. The sea breezes survive even after sunset and converge in the center of the island before midnight, associated with heavy precipitation. The precipitation maintains its intensity until early morning.

The results may depend on the planetary boundary-layer scheme and land-surface scheme chosen; however, the results of sensitivity experiments using two other planetary-boundary layer schemes (YSU and MRF) and another land-surface scheme (RUC) demonstrate that the results do not strongly depend on the scheme used.

3.3. Mechanism of the diurnal cycle of convective activities over the Borneo Island

Arakawa and Kitoh (2005) reported that the MRI-GCM could roughly simulate the features of local circulation generated by the orography. In our results, the phase of the diurnal cycle of precipitation simulated by the MRI-GCM also agrees well with that of the TRMM-NSR over small islands and straits whose horizontal scale is less than 200 km. However, the phase of the diurnal variation exhibits a large discrepancy between the simulated and observed precipitation around large islands such as Sumatra, Borneo, and New Guinea.

Previous studies using GCMs with coarse grid spacing generally indicated that the simulated precipitation occurs earlier and continues for a shorter time than the observed one (e.g. Neale and Slingo 2003; Collier 2004; Dai 2006). Lee et al. (2007b) stated that the diurnal cycle strongly depends on the parameters of the cumulus parameterization.

In the simulation by the MRI-GCM, more than 80 % of the total precipitation around the

Maritime Continent is due to the Arakawa-Schubert-type cumulus convective parameterization scheme. The precipitation caused by the cumulus parameterization scheme is sensitive to daytime instability in the lower atmosphere because of surface solar heating. As a result, parameterization tends to yield the most precipitation in the late afternoon over the land surface on clear days. The model accurately simulates the manner in which convection is generated over a mountain range or near the coast from the afternoon to the evening, but the simulated convection system does not propagate inland and finishes earlier than the ones observed, in addition to yielding a discontinuous phase distribution across the western coast of Sumatra.

The diurnal variation of precipitation is not simulated well around Borneo Island. The MRI-GCM incompletely simulates the nocturnal convection propagating offshore. This propagation was first found by Houze et al. (1981). Over the inland area, the simulated precipitation has a very large phase error in the diurnal cycle. The inland propagation of convection is not simulated at all. Although the model accurately simulates the convection system generated near the coast in the afternoon, the simulated convection does not propagate inland and finishes much earlier than it does in the observation.

The discrepancy in the phase distribution between most GCMs and the corresponding observations may be partially caused by lower resolution, as a result of which the model may not adequately simulate thermally induced local circulations that enhance the generation of convection systems. Many previous studies (Kimura and Kuwagata 1995; Sato and Kimura 2005; Simpson 1994, etc.) showed that local circulations often induce convection. The local circulations maintain and sometimes enhance the static instability after sunset and even as late as midnight and contribute to the late precipitation. The mechanisms of the diurnal cycle of precipitation revealed by previous studies are summarized as follows: 1) development of convective storms over a sea-breeze front (e.g. Pielke 1974), 2) moisture conversion over mountains by upslope winds (Sato and Kimura 2005), 3) propagation of multi-cell convective storms from the mountains (e.g. Satomura 2000), and 4) interaction

of convective storms with monsoon and/or land-sea breeze (Houze et al. 1981). Kimura and Kuwagata (1995) studied the moisture transport toward mountains using their simple non-condensation model and stated that the phase and magnitude of the diurnal cycle of the transport depend on the horizontal scale of the mountains. Larger horizontal scales yield later maximum precipitation. The vertical integrated moisture reaches its maximum in the early evening when the horizontal scale is about 80 to 160 km. These moisture cycles may affect the precipitation there. Neale and Slingo (2003) suggested that a coarse-mesh simulation, in which local circulations cannot be simulated in detail, causes phase errors in diurnal variations in GCMs. However, such differences in precipitation are still found even in a high-resolution simulation by the MRI-GCM, which would be expected to represent local-scale circulations, or at least the most effective ones with a horizontal scale of 80 to 160 km.

Another reason for the discrepancy between the MRI-GCM and the observation is the propagation of the MCSs. Nesbitt and Zipser (2003) and Hirose (2005) analyzed TRMM data and stated that strong precipitation zones were induced by organized MCSs, for example, a multi-cell-type storm (Houze 1993). Tompkins (2001) studied the organization process of tropical convection over the ocean. Using a high-resolution, cloud-resolving model, he clarified that the cold pool produced by deep convection becomes a trigger for the next generation of convections and plays an important role in the spatial organization of tropical deep convection. Although his experiments were limited to the situation of weak, large-scale wind shear and a homogeneous sea-surface temperature, this effect can partially explain the propagation of convection over the ocean, particularly to the west of Sumatra Island.

On Borneo Island, for example, systematic propagation can be observed that are well synchronized with the diurnal cycle. The convection system obviously propagates from the coasts inland, as seen in Fig. 3.4, and as a result the time of the maximum precipitation strongly depends on the distance from the coast. Previous studies suggest that nighttime convection is related to both self-organization of the convection and local circulation around

the islands (Ichikawa and Yasunari 2006; Williams and Houze 1987). The non-hydrostatic model indicates that local circulations can easily induce convection areas over the land surface, especially over mountain ranges or coastal areas in the late afternoon. The convection systems then propagate inland. Although the mechanism of the propagation is not made entirely clear by these model studies, it can be assumed to contain two important processes. One is the self-organization of convection, including the evolution of a cold pool, and the other is forcing by the local circulations. As previously mentioned, simulated precipitation bands intrude into inland areas associated with wind systems that seem to be sea-breeze fronts. Since the sea-breeze fronts are also expected to be modified by the precipitation, these two should interact non-linearly. Simpson (1994) showed that the observed sea breeze had a quite large horizontal scale (more than two hundred kilometers) and longer life (more than twelve hours) in some places. These facts are not in conflict with previous theoretical studies (Dalu and Pielke 1989), but the non-linear interaction may also be related to such characteristics.

3.4. Conclusions

Recent studies using GMS and TRMM data revealed that a diurnal cycle is prominent in precipitation around the Maritime Continent and contributes to most of the total precipitation. MRI-GCM can simulate convection systems with a prominent diurnal cycle around the Maritime Continent. However, there are some differences in the spatial distribution and in the phase of the diurnal cycle between the simulated precipitation and that observed by the TRMM-NSR.

The spatial distributions of the total amount and amplitude of the diurnal cycle of the simulated precipitation agree quite well with the observation for small islands, i.e., those with a 100 to 200 km width. In contrast, the MRI-GCM did not simulate well the process and structures of convection systems over large islands whose width exceeds 200 km. The phase difference in the diurnal cycle of precipitation between the TRMM-NSR and the MRI-GCM

often reaches about 12 hours for large islands such as Borneo and New Guinea. Over the western offshore of Sumatra, the difference in the peak time of the diurnal precipitation cycle between the observation and simulation is small, but the difference in the total precipitation is large. Specifically, there is an underestimation of nearly 2000 mm/year over the area. The westward propagation of the precipitation system cannot be simulated, and the duration of precipitation is much shorter than that in the observation.

The grid spacing of the MRI-GCM, 20 km, is fine enough to resolve the topography and the major thermally induced local circulations, which seem to drive the diurnal cycle of precipitation. However, the model does not always simulate the process and structures of the diurnal cycle of the convection systems. The reason for this could be that the MRI-GCM cannot simulate the coupling between a self-organized convection system and the local circulation because a cumulus convective parameterization is adopted. The two systems are strongly and non-linearly coupled through many processes, such as the distribution of moist instability, triggers for deep convections, and the formation of cold pools by rainfall.

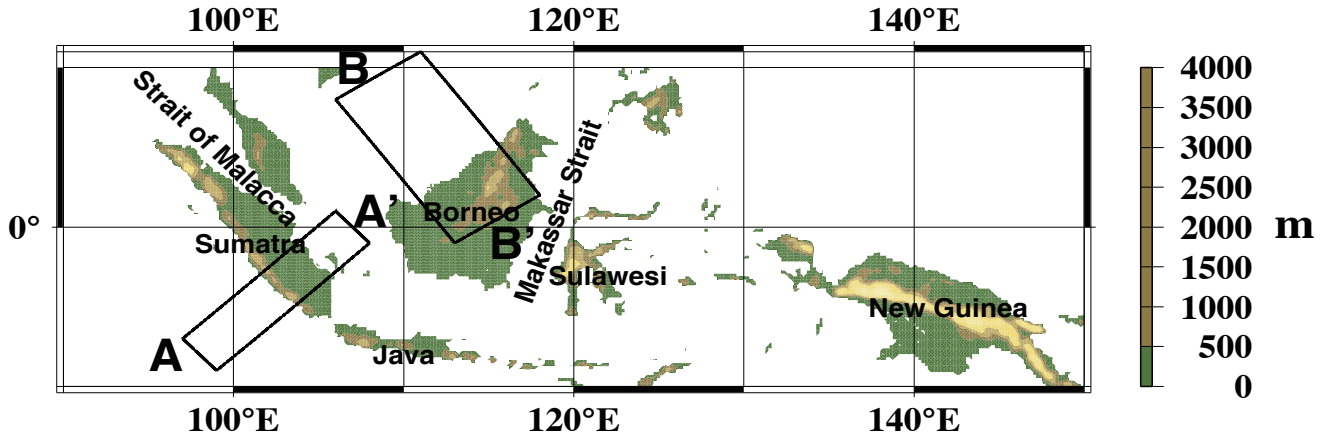

FIG. 3.1. Topography used in the MRI-GCM simulation over the Maritime continent.

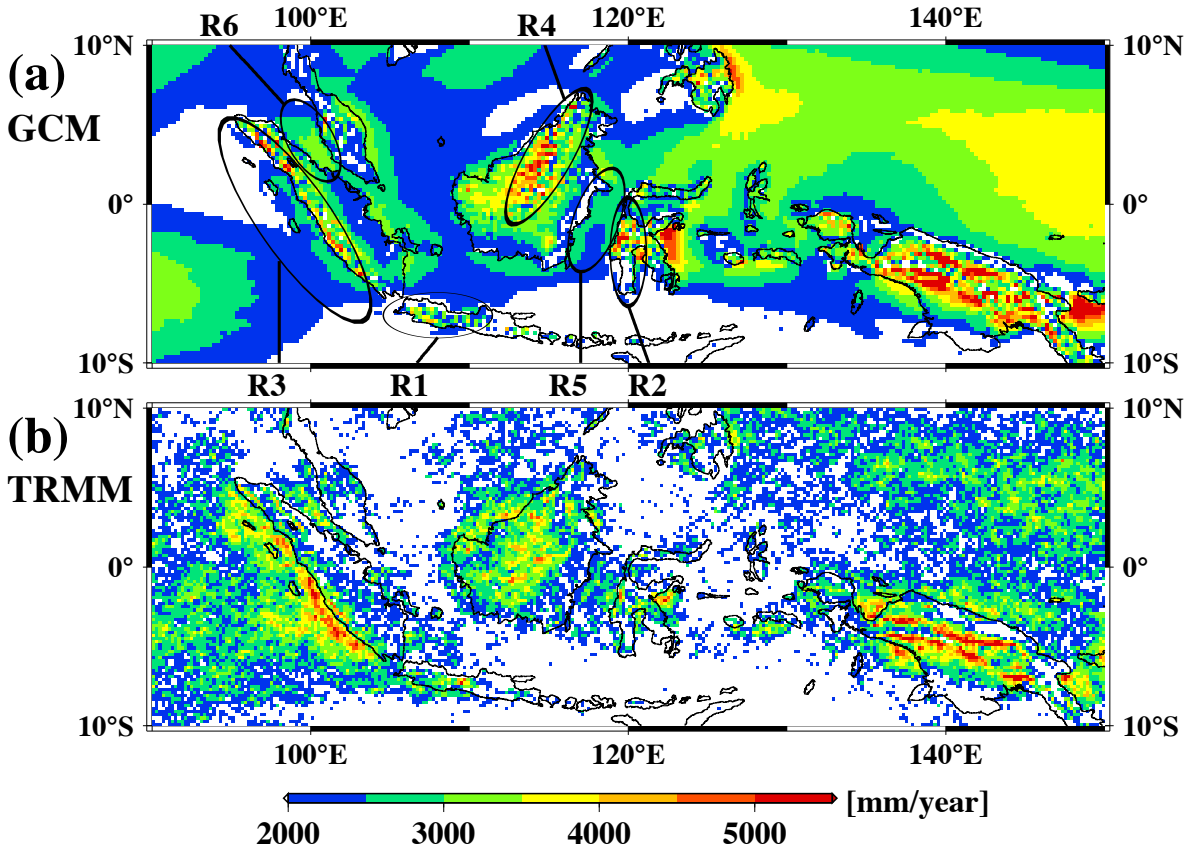

FIG. 3.2. Annual precipitation over the Maritime Continent by (a) ten-year-averaged MRI-GCM and (b) eight-year-averaged TRMM-NSR.

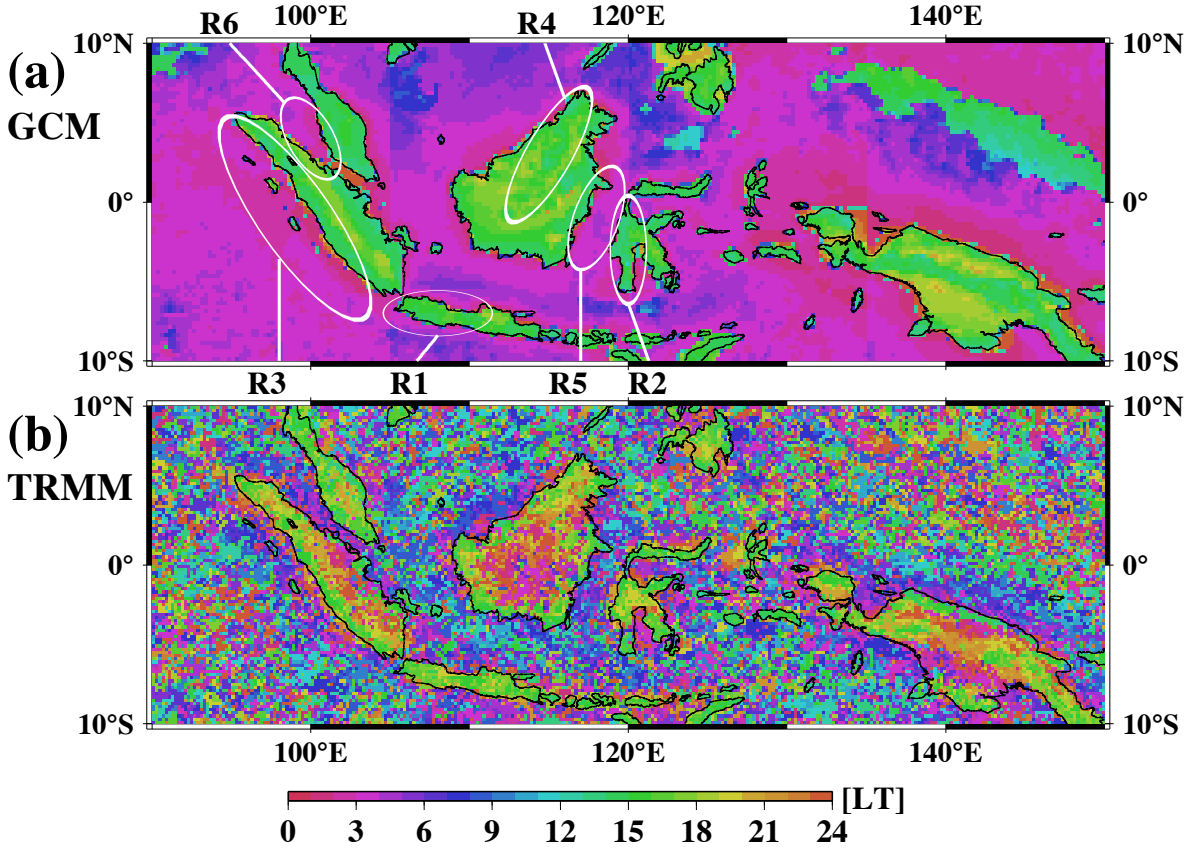

FIG. 3.3. Maximum precipitation time (local time) by (a) MRI-GCM and (b) TRMM-NSR.

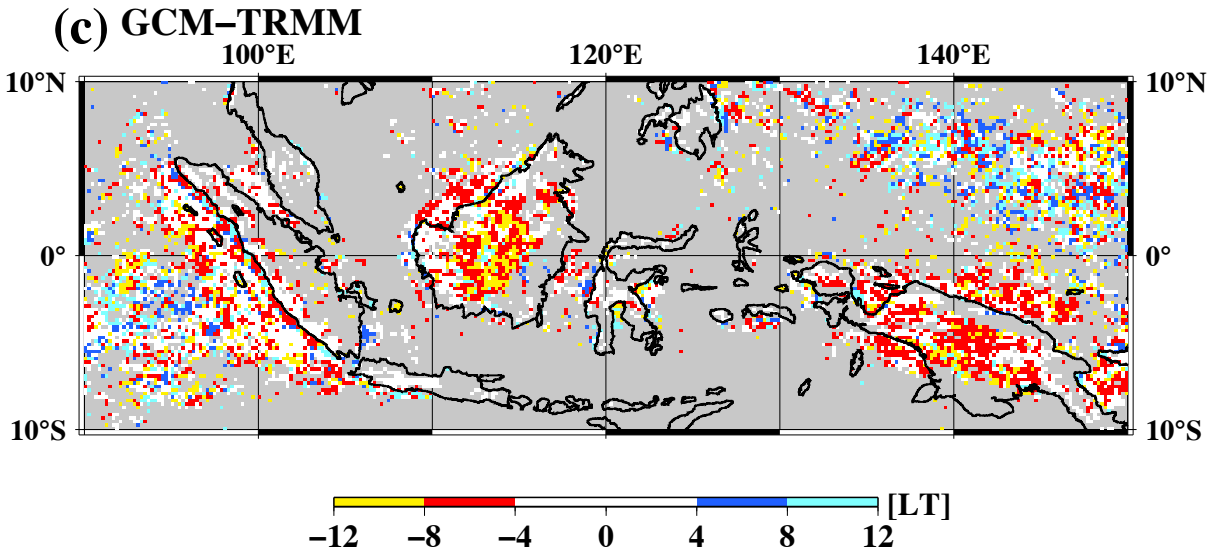

FIG. 3.4. Difference of maximum precipitation time (local time) by MRI-GCM and TRMM-NSR. Areas in which the eight-year-averaged annual precipitation observed by TRMM-NSR is less than 2500 mm/year are masked out.

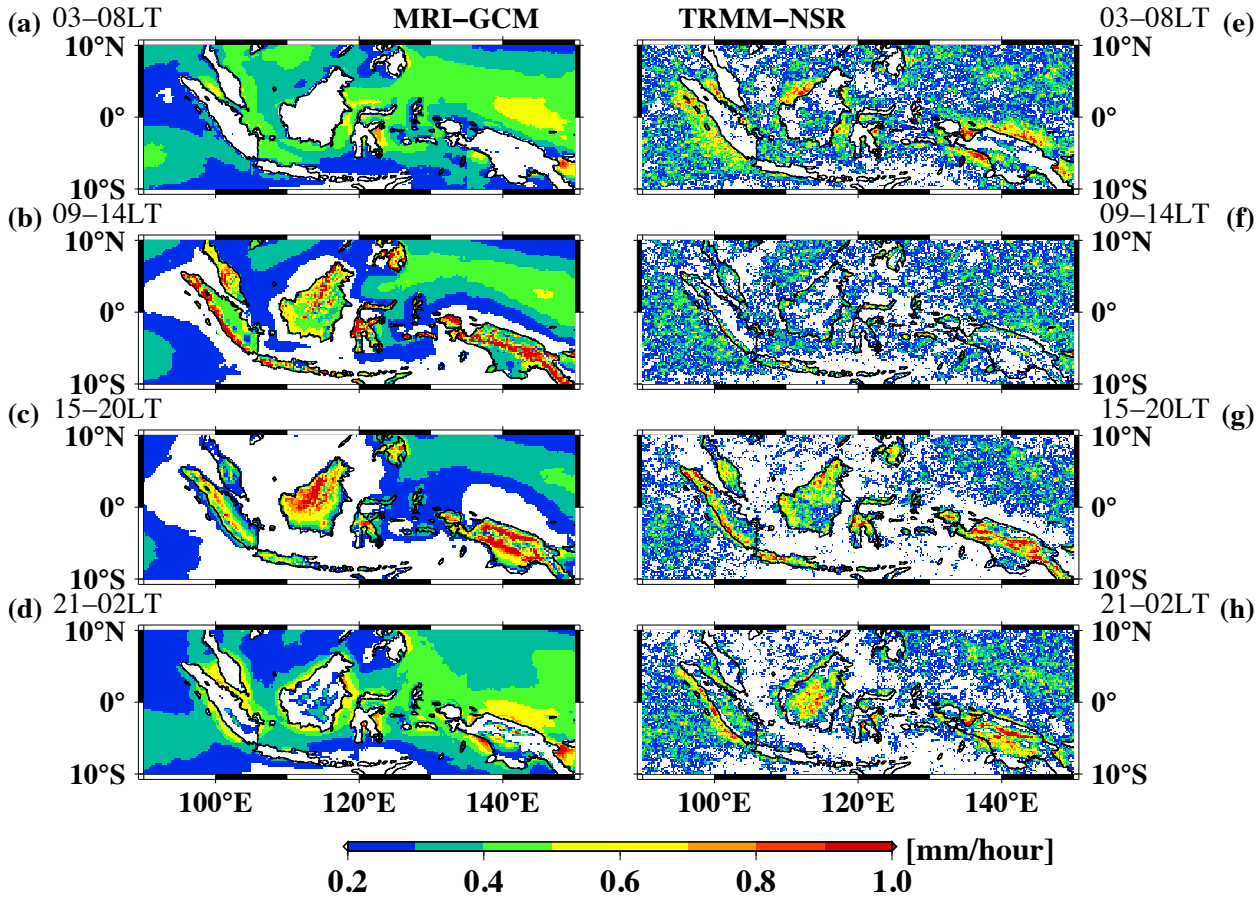

FIG. 3.5. Six-hourly precipitation over the Maritime Continent by (a) MRI-GCM, (b) TRMM-NSR.

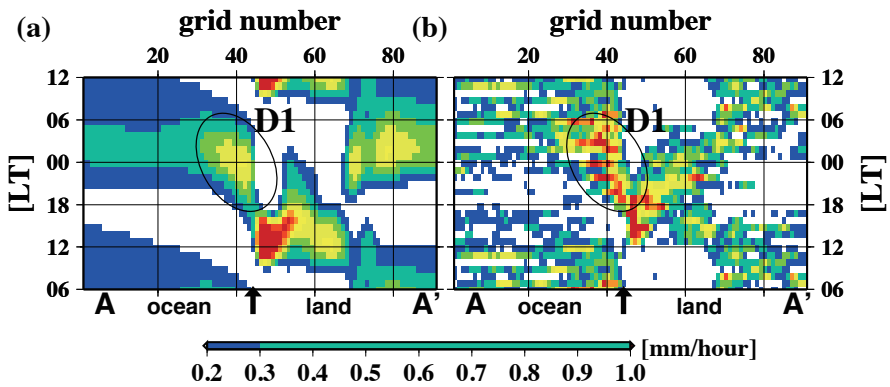

FIG. 3.6. Distance-time cross-section of the precipitation along belt A-A' in Fig. 3.1 by (a) MRI-GCM and (b) TRMM-NSR. The arrows indicate the location of the coastline.

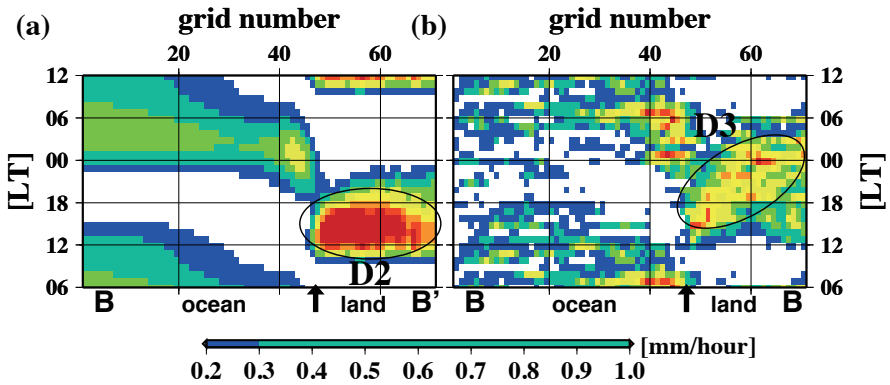

FIG. 3.7. As in Fig. 3.6, but along belt B-B'.

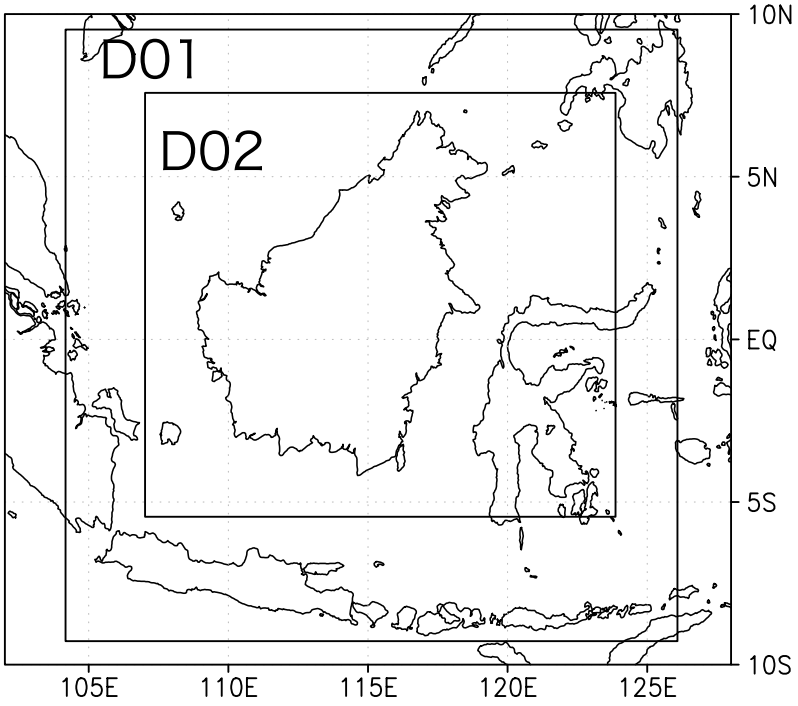

FIG. 3.8. Domains of simulations used in the regional climate model.

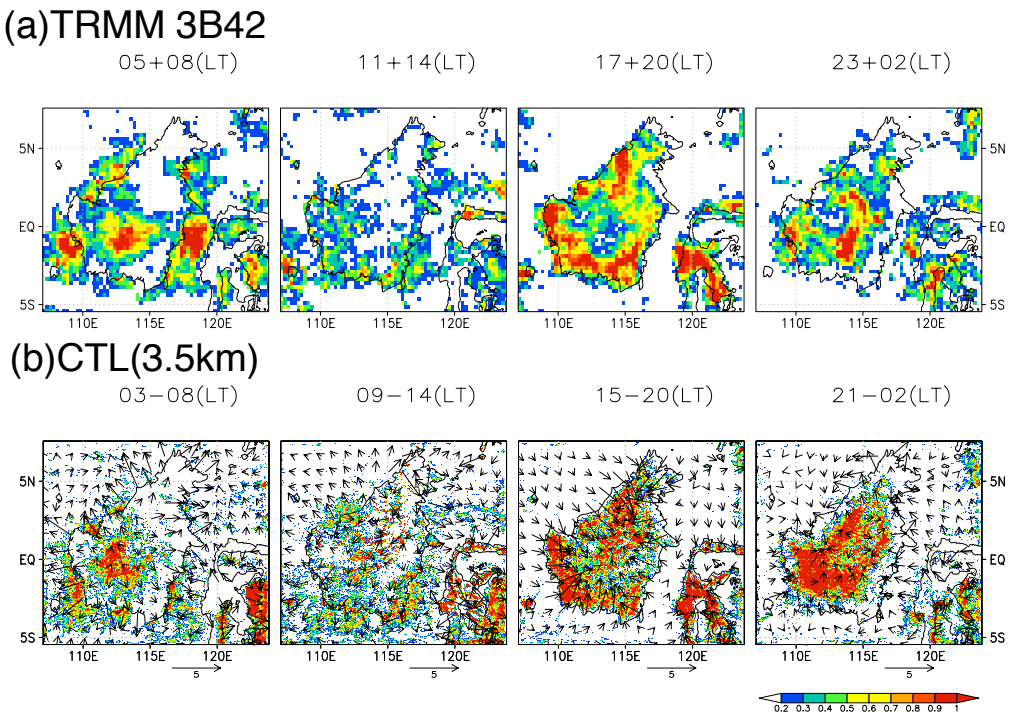

FIG. 3.9. One-month averaged six-hourly precipitation over the Maritime Continent by (a) TRMM-3B42 and (b) WRF simulation. The arrows indicate the deviations of simulated horizontal winds.

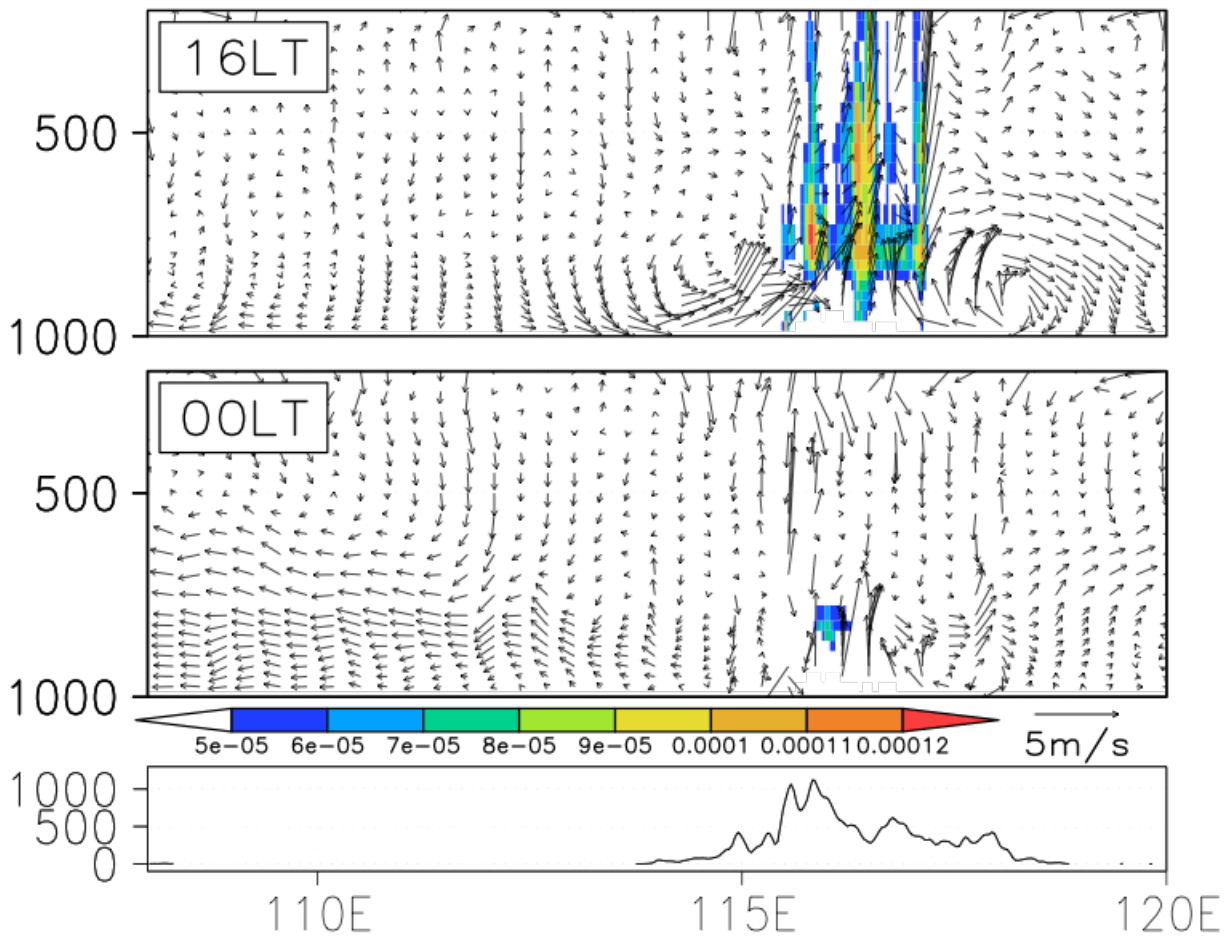

Fig. 3.10. Longitude-height cross section of monthly averaged mixing ratio of liquid and ice (shade) and longitudal and vertical wind (vector) at 16 LST (upper panel) and 00 LST (middle panel) at 4 °N. Wind is deviation from mean state. The vertical wind is magnified a hundred times. Vertical axis of upper and middle panels are in hPa. Lower panel shows orographic height. Vertical axis of lower panel is in meter.

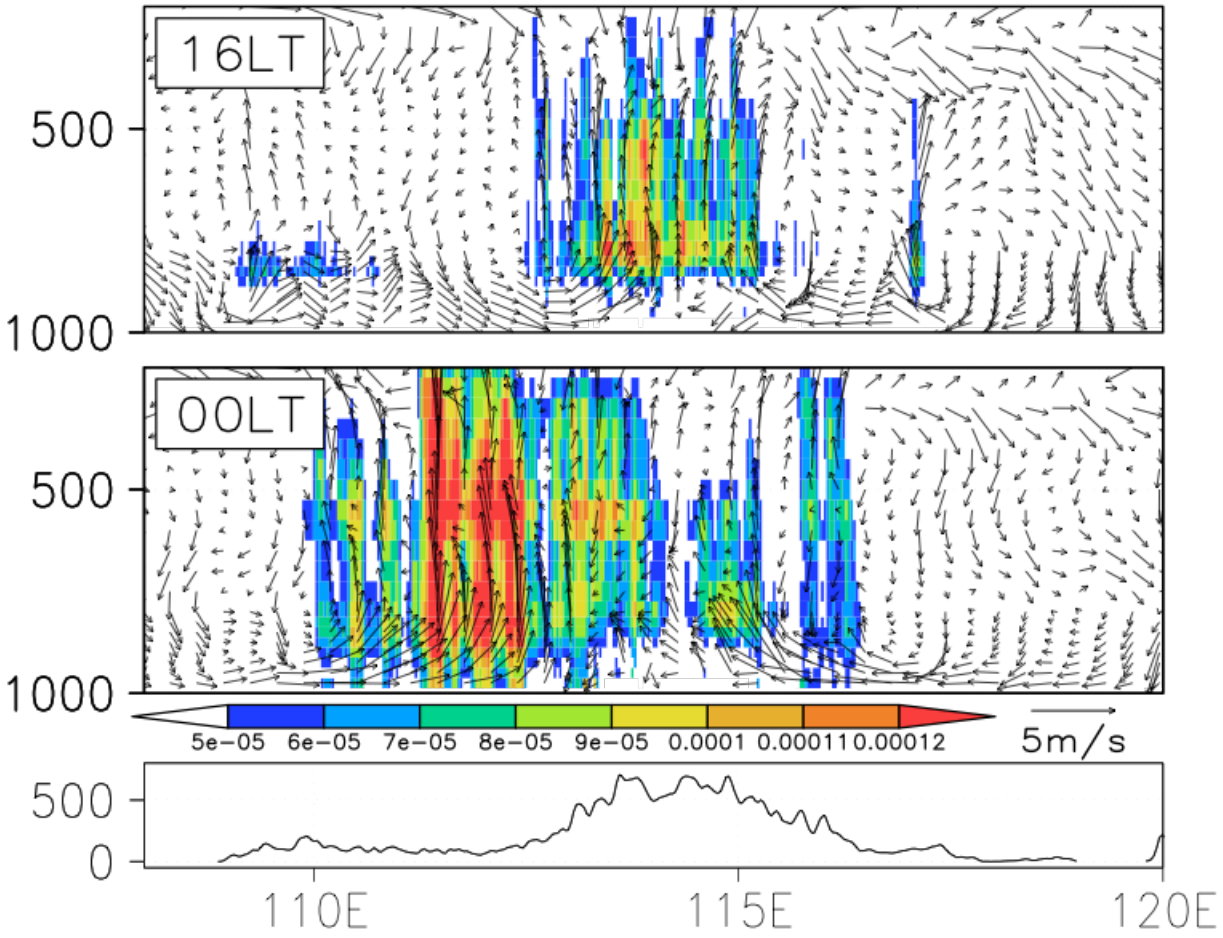

FIG. 3.11. Same as Fig. 3.10, but for at the equator.

Chapter 5

CONCLUSIONS

In this paper, we have conducted a series of dynamical downscaling studies over the Asia region and developed a new regional climate model based on a global cloud-resolving atmospheric model. Our targets are the regional climate strongly influenced by surface conditions, (i.e., topographic features and land cover), cumulus convection, and local circulation. In the first two studies, our target is the future regional climate in Japan. We have studied snow and the urban heat island of regional future climate change using the dynamical downscaling method.

First, the 2070s snow water equivalent in cases of much and little snow is projected by the WRF model using the PGW method. We also performed present climate simulations in cases of much and little snow. The precipitation amount is almost the same in present and future climates, but the snow water equivalent is remarkably decreased because snowfall changes into rainfall and fallen snow melts due to the rise in air temperature. The projected maximum snow depth can decrease about 50 % in high snow cases and 70 % in low snow cases in the 2070s. The decrease is remarkable in the lowland, where the orographic height is less than 500 m. Thus, the result shows that the future snow change can be strongly affected by detailed topographic features. Second, we have conducted a couple of numerical experiments targeting the wintertime urban heat island around the Tokyo metropolitan area. The Tokyo metropolitan area is one of the largest urban areas in the world. This study investigates the change in urban heat island intensity of the Tokyo metropolitan area in winter

by the effects of global climate change. We performed present and future climate simulations using a regional climate model, the Weather Research and Forecasting (WRF) model, including an urban canopy sub-model (Kusaka et al., 2001). Future climate simulation was conducted using pseudo-global-warming (PGW) method (Kimura and Kitoh, 2008), assuming the boundary conditions estimated by CMIP3 GCMs under the SRES scenarios. The PGW method is a useful method for future downscaling and is adopted for some studies on urban heat islands (Kusaka et al., 2012) and winter climate (Hara et al., 2008) over Japan. The simulation results indicated that UHII would be enhanced during the night due to the global climate change. The urban thermal environment study shows that the warming due to urbanization and that due to global warming are almost the same (about three degrees) in the 2070s, although the urban heat island intensity can be higher in the future. Detailed land cover utilized in dynamical downscaling is essential to represent such an urban thermal environment.

Third, we analyzed the diurnal cycle of convective activity over the Maritime Continent using a 20-km mesh GCM. The results show the systematic error due to cumulus convective parameterization and a large grid size. To elucidate the mechanism of the diurnal cycle of convective activity and the systematic error, we performed one-month simulations during an absent MJO season using the WRF model. The spatial distribution and time evolution of the simulated diurnal cycle of convection are in accordance with the GMS and TRMM data. In the northern part of Borneo Island, the distance from the coastline to the central mountains is relatively narrow (about 100 km), while the distance is relatively broad (about 500 km) in the southern part of Borneo Island. Over the northern part of Borneo Island, land-sea breeze and upslope wind develop and convection initiates only over mountainous areas. The convective activities over the mountainous areas decay in the evening. Over the southern part of Borneo Island, sea breeze and upslope wind develop separately in the afternoon, and convective activities occur over sea breeze fronts and mountainous areas. Between the sea breeze fronts and mountainous areas, convective activities are suppressed by compensational

subsidence. In the evening, the sea breeze front penetrates into inland areas and couples with convection over mountainous areas, and the convective activities continue until the next morning. The diurnal cycle of convective activity over Borneo Island is maintained by the sea breeze and upslope wind, and it depends on the distance from the coastline to the central mountains. There is room for further investigation regarding the dependency of spatial scale and land-sea contrast for convective activity.

Finally, we developed and verified a diamond NICAM based on global NICAM. The diamond NICAM we developed is based on the original NICAM. To verify the geometric structure, especially in the lateral boundary of a diamond, of the diamond NICAM, we performed a test simulation based on Williamson et al. (1992), using a shallow-water version of the diamond NICAM. Results from the diamond NICAM show good agreement with the global NICAM simulation. After that, we examined the realistic one-month simulation using the diamond NICAM with full physics. The simulation results show that the diamond NICAM has almost the same simulatability as the stretched NICAM and global NICAM results.

The diamond NICAM we developed has the same physics schemes and dynamical framework as the original NICAM. We can use long-term simulation of the global NICAM as lateral boundary data for the diamond NICAM simulation to perform dynamical downscaling. When we use the diamond NICAM as a regional climate model, uncertainty caused by the discrepancy between GCMs and RCMs can be reduced because the physical process schemes and dynamical framework used in the global NICAM and the diamond NICAM are identical.

Acknowledgments

I would like to express my special gratitude to Prof. Hiroyuki Kusaka and Prof. Fujio Kimura, who encourage and supervise my whole research activities. I am indebted to thank Prof. Hiroshi L. Tanaka, Prof. Teruyuki Kato, Prof. Yasutaka Wakazuki, and colleagues in JAMSTEC and University of Tsukuba, who improved my analysis methods and helped to broaden the perspective of research, for valuable comments and suggestions.

I wish to acknowledge to valuable discussions with Dr. Yuya Takane, Mr. Ryosaku Ikeda, Ms Yuko Akimoto, Dr. Maki Okada, Mr. Takayuki Kato, Mr. Akifumi Nishi whose for their encouraging comments on my study and oral examination.

Finally, I also acknowledge my gratitude to my parents for their great supports at various points in my life. My appreciation to them is beyond describable.

References

Adachi, S. A., F. Kimura, H. Kusaka, T. Inoue, and H. Ueda, 2012: Comparison of the impact of global climate changes and urbanization on summertime future climate in the Tokyo metropolitan area. *Journal of Applied Meteorology and Climatology*, **51 (8)**, 1441–1454, doi:10.1175/JAMC-D-11-0137.1.

Anthes, R., E.-Y. Hsie, and Y.-H. Kuo, 1986: Description of the Penn State/NCAR Mesoscale Model: Version 4 (MM4). Tech. rep., National Center for Atmospheric Research, 66 pp., CO, USA. doi:10.5065/D64B2Z90.

Anthes, R. A., 1990: Recent applications of the Penn State/NCAR Mesoscale Model to synoptic, mesoscale, and climate studies. *Bulletin of the American Meteorological Society*, **71 (11)**, 1610–1629, doi:10.1175/1520-0477(1990)071⟨1610:RAOTPS⟩2.0.CO;2.

Arakawa, O. and A. Kitoh, 2005: Rainfall diurnal variation over the Indonesian maritime continent simulated by 20 km-mesh GCM. *SOLA*, **1**, 109–112, doi:10.2151/sola.2005-029.

Boorman, P., G. Jenkins, J. Murphy, and K. Burgess, 2010: Future changes in lightning from the UKCP09 ensemble of regional climate model projections. Tech. rep., UKCP, 24 pp., United Kingdom.

Brown, S., P. Boorman, R. McDonald, and J. Murphy, 2009: Interpretation for use of surface wind speed projections from the 11-member Met Office Regional Climate Model ensemble. Tech. rep., UKCP, 24 pp., United Kingdom.

Brown, S., P. Boorman, and J. Murphy, 2010: Interpretation and use of future snow projections from the 11-member Met Office Regional Climate Model ensemble. Tech. rep., UKCP, 25 pp., United Kingdom.

Chen, F. and J. Dudhia, 2001: Coupling an advanced land surface-hydrology model with the Penn State-NCAR MM5 modeling system. Part I: Model implementation and sensitivity. *Monthly Weather Review*, **129 (4)**, 569–585, doi:10.1175/1520-0493(2001)129⟨0569:CAALSH⟩2.0.CO;2.

Chen, F., et al., 2011: The integrated WRF/urban modelling system: development, evaluation, and applications to urban environmental problems. *International Journal of Climatology*, **31 (2)**, 273–288, doi:10.1002/joc.2158.

Cohen, S. J., 1990: Bringing the global warming issue closer to home: The challenge of regional impact studies. *Bulletin of the American Meteorological Society*, **71 (4)**, 520–526, doi:10.1175/1520-0477(1990)071⟨0520:BTGWIC⟩2.0.CO;2.

Collier, J. C., 2004: Diurnal cycle of tropical precipitation in a general circulation model. *Journal of Geophysical Research*, **109 (D17)**, D17 105, doi:10.1029/2004JD004818.

Côté, J., S. Gravel, A. Méthot, A. Patoine, M. Roch, and A. Staniforth, 1998: The operational CMC-MRB global environmental multiscale (GEM) model. Part I: Design considerations and formulation. *Monthly Weather Review*, **126 (6)**, 1373–1395, doi:10.1175/1520-0493(1998)126⟨1373:TOCMGE⟩2.0.CO;2.

Dai, A., 2006: Precipitation characteristics in eighteen coupled climate models. *Journal of Climate*, **19 (18)**, 4605–4630, doi:10.1175/JCLI3884.1.

Dai, A. and K. E. Trenberth, 2004: The diurnal cycle and its depiction in the community climate system model. *Journal of Climate*, **17 (5)**, 930–951, doi:10.1175/1520-0442(2004)017⟨0930:TDCAID⟩2.0.CO;2.

Dalu, G. A. and R. A. Pielke, 1989: An analytical study of the sea breeze. *Journal of the Atmospheric Sciences*, **46 (12)**, 1815–1825, doi:10.1175/1520-0469(1989)046⟨1815:AASOTS⟩2.0.CO;2.

Déqué, M. and J. P. Piedelievre, 1995: High resolution climate simulation over Europe. *Climate Dynamics*, **11 (6)**, 321–339, doi:10.1007/BF00215735.

Dickinson, R., R. Errico, F. Giorgi, and G. Bates, 1989: A regional climate model for the western United States. *Climatic Change*, **15 (3)**, doi:10.1007/BF00240465.

Emori, S., T. Nozawa, A. Numaguti, and I. Uno, 2001: Importance of cumulus parameterization for precipitation simulation over east Asia in June. *Journal of the Meteorological Society of Japan*, **79 (4)**, 939–947, doi:10.2151/jmsj.79.939.

Fox-Rabinovitz, M. S., J. Côté, B. Dugas, M. Déqué, and J. L. McGregor, 2006: Variable resolution general circulation models: Stretched-grid model intercomparison project (SGMIP). *Journal of Geophysical Research*, **111 (D16)**, D16 104, doi:10.1029/2005JD006520.

Fox-Rabinovitz, M. S., L. L. Takacs, R. C. Govindaraju, and M. J. Suarez, 2001: A variable-resolution stretched-grid general circulation model: regional climate simulation. *Monthly Weather Review*, **129 (3)**, 453–469, doi:10.1175/1520-0493(2001)129⟨0453:AVRSGG⟩2.0.CO;2.

Giorgi, F., 1990: Simulation of regional climate using a limited area model nested in a general circulation model. *Journal of Climate*, **3 (9)**, 941–963, doi:10.1175/1520-0442(1990)003⟨0941:SORCUA⟩2.0.CO;2.

Giorgi, F., 1991: Sensitivity of simulated summertime precipitation over the western United States to different physics parameterizations. *Monthly Weather Review*, **119 (12)**, 2870–2888, doi:10.1175/1520-0493(1991)119⟨2870:SOSSPO⟩2.0.CO;2.

Giorgi, F. and G. T. Bates, 1989: The climatological skill of a regional model over complex terrain. *Monthly Weather Review*, **117**, 2325–2347, doi:10.1175/1520-0493(1989)117⟨2325: TCSOAR⟩2.0.CO;2.

Giorgi, F. and L. O. Mearns, 1991: Approaches to the simulation of regional climate change: A review. *Reviews of Geophysics*, **29 (2)**, 191, doi:10.1029/90RG02636.

Hara, M., H. Kusaka, F. Kimura, and Y. Wakazuki, 2010: Effect of global climate change on urban heat island intensity of Tokyo metropolitan area – winter season case –. *Nagare*, **29 (5)**, 353–361.

Hara, M., T. Yoshikane, H. Kawase, and F. Kimura, 2008: Estimation of the impact of global warming on snow depth in Japan by the pseudo-global-warming method. *Hydrological Research Letters*, **2**, 61–64, doi:10.3178/hrl.2.61.

Hirose, M., 2005: Spatial and diurnal variation of precipitation systems over Asia observed by the TRMM precipitation radar. *Journal of Geophysical Research*, **110 (D5)**, D05 106, doi:10.1029/2004JD004815.

Hong, S.-Y. and M. Kanamitsu, 2014: Dynamical downscaling: Fundamental issues from an NWP point of view and recommendations. *Asia-Pacific Journal of Atmospheric Sciences*, **50 (1)**, 83–104, doi:10.1007/s13143-014-0029-2.

Hosaka, M., D. Nohara, and A. Kitoh, 2005: Changes in snow cover and snow water equivalent due to global warming simulated by a 20km-mesh global atmospheric model. *SOLA*, **1**, 93–96, doi:10.2151/sola.2005-025.

Houze, R. A., 1993: *Cloud dynamics, Volume 53*. Academic Press, 573 pp.

Houze, R. A., S. G. Geotis, F. D. Marks, and A. K. West, 1981: Winter monsoon convection in the vicinity of north borneo. Part I: Structure and time variation of the clouds and

precipitation. *Monthly Weather Review*, **109 (8)**, 1595–1614, doi:10.1175/1520-0493(1981)109⟨1595:WMCITV⟩2.0.CO;2.

Huffman, G. J., et al., 2007: The TRMM multisatellite precipitation analysis (TMPA): Quasi-global, multiyear, combined-sensor precipitation estimates at fine scales. *Journal of Hydrometeorology*, **8 (1)**, 38–55, doi:10.1175/JHM560.1.

Ichikawa, H. and T. Yasunari, 2006: Time-space characteristics of diurnal rainfall over Borneo and surrounding oceans as observed by TRMM-PR. *Journal of Climate*, **19 (7)**, 1238–1260, doi:10.1175/JCLI3714.1.

Ichinose, T., K. Shimodozono, and K. Hanaki, 1999: Impact of anthropogenic heat on urban climate in Tokyo. *Atmospheric Environment*, **33 (24-25)**, 3897–3909, doi:10.1016/S1352-2310(99)00132-6.

Intergovernmental Panel on Climate Change, 1990: *Climate change: The IPCC scientific assessment*. Cambridge University Press, Cambridge, United Kingdom and New York, NY, USA, 410 pp.

Intergovernmental Panel on Climate Change, 2000: *Special report on emissions scenarios: A special report of working group III of the intergovernmental panel on climate change*. Cambridge University Press, Cambridge, United Kingdom, 570 pp.

Intergovernmental Panel on Climate Change, 2007: *Climate change 2007: The physical science basis*. 1st ed., Cambridge University Press, Cambridge, United Kingdom and New York, NY, USA, 996 pp.

Japan Meteorological Agency, 2001: Global warming projection Vol. 4.

Japan Meteorological Agency, 2003: Global warming projection Vol. 5.

Japan Meteorological Agency, 2004: Heat island monitoring report: Kanto district in summer, 2003.

Japan Meteorological Agency, 2005: Global warming projection Vol. 6.

Japan Meteorological Agency, 2008: Global warming projection Vol. 7.

Japan Meteorological Agency, 2012: Heat island monitoring report.

Japan Meteorological Agency, 2013: Global warming projection Vol. 8.

Jones, R. G., J. M. Murphy, and M. Noguer, 1995: Simulation of climate change over europe using a nested regional-climate model. I: Assessment of control climate, including sensitivity to location of lateral boundaries. *Quarterly Journal of the Royal Meteorological Society*, **121 (526)**, 1413–1449, doi:10.1002/qj.49712152610.

Kalnay, E., et al., 1996: The NCEP/NCAR 40-year reanalysis project. *Bulletin of the American Meteorological Society*, **77 (3)**, 437–471, doi:10.1175/1520-0477(1996)077⟨0437:TNYRP⟩2.0.CO;2.

Kato, H., 1999: Recent progress on regional climate modeling studies. *Gekkan Kaiyo*, **4**, 81–89.

Kawase, H., T. Yoshikane, M. Hara, F. Ailikun, Borjigint eand Kimura, and T. Yasunari, 2008: Downscaling of the climatic change in the rainband in east asia by a pseudo climate simulation method. *Scientific Online Letters on the Atmosphere*, **4**, 73–76, doi:10.2151/sola.2008-019.

Kawase, H., T. Yoshikane, M. Hara, M. Fujita, N. Ishizaki, , F. Kimura, and H. Hatsushika, 2012: Downscaling of snow cover changes in the late 20th century using a past climate simulation method over central japan. *Scientific Online Letters on the Atmosphere*, **8**, 61–64, doi:10.2151/sola.2012-016.

Kawase, H., T. Yoshikane, M. Hara, F. Kimura, T. Yasunari, B. Ailikun, H. Ueda, and T. Inoue, 2009: Intermodel variability of future changes in the Baiu rainband estimated

by the pseudo global warming downscaling method. *Journal of Geophysical Research*, **114 (D24)**, D24 110, doi:10.1029/2009JD011803.

Kida, H., T. Koide, H. Sasaki, and M. Chiba, 1991: A new approach for coupling a limited area model to a GCM for regional climate simulations. *Journal of the Meteorological Society of Japan. Ser. II*, **69 (6)**, 723–728.

Kimura, F. and A. Kitoh, 2007: Downscaling by pseudo global warming method, the final report of the ICCAP. Tech. rep., Research Institute for Human and Na ture (RIHN), Kyoto, Japan.

Kimura, F. and T. Kuwagata, 1995: Horizontal heat fluxes over complex terrain computed using a simple mixed-layer model and a numerical model. *Journal of Applied Meteorology*, **34 (2)**, 549–558, doi:10.1175/1520-0450-34.2.549.

Kimura, F. and S. Takahashi, 1991: The effects of land-use and anthropogenic heating on the surface temperature in the Tokyo Metropolitan area: a numerical experiment. *Atmospheric Environment. Part B. Urban Atmosphere*, **25 (2)**, 155–164, doi:10.1016/0957-1272(91)90050-O.

Kondo, J., 1993: A new bucket model for predicting water content in the surface soil layer. *Journal of Japan Society of Hydrology and Water Resources*, **6 (4)**, 344–349, doi:10.3178/jjshwr.6.4_344.

Kurihara, K., et al., 2005: Projection of climatic change over Japan due to global warming by high-resolution regional climate model in MRI. *SOLA*, **1**, 97–100, doi:10.2151/sola.2005-026.

Kusaka, H., 2009: About a regional atmospheric model, WRF. *Nagare*, **28**, 3–12.

Kusaka, H., M. Hara, and Y. Takane, 2012: Urban climate projection by the WRF model at 3-km horizontal grid increment: Dynamical downscaling and predicting heat stress in the

2070's August for Tokyo, Osaka, and Nagoya metropolises. *Journal of the Meteorological Society of Japan. Ser. II*, **90B**, 47–63, doi:10.2151/jmsj.2012-B04.

Kusaka, H. and F. Kimura, 2004: Coupling a single-layer urban canopy model with a simple atmospheric model: Impact on urban heat island simulation for an idealized case. *Journal of the Meteorological Society of Japan*, **82 (1)**, 67–80, doi:10.2151/jmsj.82.67.

Kusaka, H., H. Kondo, Y. Kikegawa, and F. Kimura, 2001: A simple single-layer urban canopy model for atmospheric models: Comparison with multi-layer and slab models. *Boundary-Layer Meteorology*, **101 (3)**, 329–358, doi:10.1023/A:1019207923078.

Kusunoki, S., J. Yoshimura, H. Yoshimura, A. Noda, K. Oouchi, and R. Mizuta, 2006: Change of Baiu rain band in global warming projection by an atmospheric general circulation model with a 20-km grid size. *Journal of the Meteorological Society of Japan*, **84 (4)**, 581–611, doi:10.2151/jmsj.84.581.

Lee, M.-I., et al., 2007a: An analysis of the warm-season diurnal cycle over the continental United States and northern Mexico in general circulation models. *Journal of Hydrometeorology*, **8 (3)**, 344–366, doi:10.1175/JHM581.1.

Lee, M.-I., et al., 2007b: Sensitivity to horizontal resolution in the AGCM simulations of warm season diurnal cycle of precipitation over the United States and northern Mexico. *Journal of Climate*, **20 (9)**, 1862–1881, doi:10.1175/JCLI4090.1.

Louis, J.-F., 1979: A parametric model of vertical eddy fluxes in the atmosphere. *Boundary-Layer Meteorology*, **17 (2)**, 187–202, doi:10.1007/BF00117978.

McGregor, J. L., 1997: Regional climate modelling. *Meteorology and Atmospheric Physics*, **63 (1-2)**, 105–117, doi:10.1007/BF01025367.

McGregor, J. L. and M. R. Dix, 2008: An updated description of the conformal-cubic

atmospheric model. *High resolution numerical modelling of the atmosphere and ocean*, K. Hamilton and W. Ohfuchi, Eds., Springer-Verlag, 51–75.

Mearns, L. O., F. Giorgi, P. Whetton, D. Pabon, M. Hulme, and M. Lal, 2003: Guidelines for use of climate scenarios developed from regional climate model experiments. Tech. rep., IPCC, 38 pp.

Mearns, L. O., W. Gutowski, R. Jones, R. Leung, S. McGinnis, A. Nunes, and Y. Qian, 2009: A regional climate change assessment program for north America. *Eos, Transactions American Geophysical Union*, **90 (36)**, 311–311, doi:10.1029/2009EO360002.

Mellor, G. L. and T. Yamada, 1974: A hierarchy of turbulence closure models for planetary boundary layers. *Journal of the Atmospheric Sciences*, **31 (7)**, 1791–1806, doi:10.1175/1520-0469(1974)031⟨1791:AHOTCM⟩2.0.CO;2.

Miura, H., M. Satoh, T. Nasuno, A. T. Noda, and K. Oouchi, 2007: A Madden-Julian oscillation event realistically simulated by a global cloud-resolving model. *Science (New York, N.Y.)*, **318 (5857)**, 1763–1765, doi:10.1126/science.1148443.

Mizuta, R., et al., 2006: 20-km-mesh global climate simulations using JMA-GSM model – mean climate states –. *Journal of the Meteorological Society of Japan*, **84 (1)**, 165–185, doi:10.2151/jmsj.84.165.

Mori, S., et al., 2004: Diurnal land-sea rainfall peak migration over Sumatera island, Indonesian maritime continent, observed by TRMM satellite and intensive rawinsonde soundings. *Monthly Weather Review*, **132 (8)**, 2021–2039, doi:10.1175/1520-0493(2004)132⟨2021:DLRPMO⟩2.0.CO;2.

Nakanishi, M. and H. Niino, 2006: An improved Mellor-Yamada level-3 model: Its numerical stability and application to a regional prediction of advection fog. *Boundary-Layer Meteorology*, **119 (2)**, 397–407, doi:10.1007/s10546-005-9030-8.

Nasuno, T., 2013: Forecast skill of Madden-Julian oscillation events in a global nonhydrostatic model during the CINDY2011/DYNAMO observation period. *SOLA*, **9**, 69–73, doi:10.2151/sola.2013-016.

Nasuno, T. and M. Satoh, 2011: Statistical relation between maximum vertical velocity and surface precipitation of tropical convective clouds in a global nonhydrostatic aquaplanet experiment. *Journal of the Meteorological Society of Japan*, **89 (5)**, 553–561, doi:10.2151/jmsj.2011-509.

Neale, R. and J. Slingo, 2003: The maritime continent and its role in the global climate: A GCM study. *Journal of Climate*, **16 (5)**, 834–848, doi:10.1175/1520-0442(2003)016⟨0834:TMCAIR⟩2.0.CO;2.

Nesbitt, S. W. and E. J. Zipser, 2003: The diurnal cycle of rainfall and convective intensity according to three years of TRMM measurements. *Journal of Climate*, **16 (10)**, 1456–1475, doi:10.1175/1520-0442-16.10.1456.

Noda, A. T., K. Oouchi, M. Satoh, H. Tomita, S.-i. Iga, and Y. Tsushima, 2010: Importance of the subgrid-scale turbulent moist process: cloud distribution in global cloud-resolving simulations. *Atmospheric Research*, **96 (2-3)**, 208–217, doi:10.1016/j.atmosres.2009.05.007.

Nozawa, T., T. Nagashima, T. Ogura, T. Yokohata, N. Okada, and H. Shiogama, 2007: Climate change simulations with a coupled ocean-atmosphere GCM called th e model for interdisciplinary research on climate: MIROC, CGER's Supercomputer Monograph Report. Tech. rep., Center for Global Environmental Research, National Institute for Environmental Studies, 79 pp., Tsukuba, Japan.

Oouchi, K., J. Yoshimura, H. Yoshimura, R. Mizuta, S. Kusunoki, and A. Noda, 2006: Tropical cyclone climatology in a global-warming climate as simulated in a 20 km-mesh global

atmospheric model: Frequency and wind intensity analyses. *Journal of the Meteorological Society of Japan*, **84 (2)**, 259–276, doi:10.2151/jmsj.84.259.

Pielke, R. A., 1974: A three-dimensional numerical model of the sea breezes over south Florida. *Monthly Weather Review*, **102 (2)**, 115–139, doi:10.1175/1520-0493(1974)102⟨0115:ATDNMO⟩2.0.CO;2.

Rummukainen, M., 2010: State-of-the-art with regional cliamte models. *WIREs Climate Change*, **1**, 82–96, doi:10.1002/wcc.008.

Sasaki, H., H. Kida, T. Koide, and M. Chiba, 1995: The performance of long-term integrations of a limited area model with the spectral boundary coupling method. *Journal of the Meteorological Society of Japan. Ser. II*, **73 (2)**, 165–181.

Sasaki, H., K. Kurihara, I. Takayabu, and T. Uchiyama, 2008: Preliminary experiments of reproducing the present climate using the non-hydrostatic regional climate model. *SOLA*, **4**, 25–28, doi:10.2151/sola.2008-007.

Sasaki, H., A. Murata, M. Hanafusa, M. Oh'izumi, and K. Kurihara, 2012: Projections of future climate change in a non-hydrostatic regional climate model nested within an atmospheric general circulation model. *SOLA*, **8**, 53–56, doi:10.2151/sola.2012-014.

Sato, T. and F. Kimura, 2005: Diurnal cycle of convective instability around the central mountains in Japan during the warm season. *Journal of the Atmospheric Sciences*, **62 (5)**, 1626–1636, doi:10.1175/JAS3423.1.

Sato, T., F. Kimura, and A. Kitoh, 2007: Projection of global warming onto regional precipitation over Mongolia using a regional climate model. *Journal of Hydrology*, **333 (1)**, 144–154, doi:10.1016/j.jhydrol.2006.07.023.

Sato, T., H. Miura, M. Satoh, Y. N. Takayabu, and Y. Wang, 2009: Diurnal cycle of pre-

cipitation in the tropics simulated in a global cloud-resolving model. *Journal of Climate*, **22 (18)**, 4809–4826, doi:10.1175/2009JCLI2890.1.

Satoh, M., 2002: Conservative scheme for the compressible nonhydrostatic models with the horizontally explicit and vertically implicit time integration scheme. *Monthly Weather Review*, **130 (5)**, 1227–1245, doi:10.1175/1520-0493(2002)130⟨1227:CSFTCN⟩2.0.CO;2.

Satoh, M., 2003: Conservative scheme for a compressible nonhydrostatic model with moist processes. *Monthly Weather Review*, **131 (6)**, 1033–1050, doi:10.1175/1520-0493(2003)131⟨1033:CSFACN⟩2.0.CO;2.

Satoh, M., T. Inoue, and H. Miura, 2010: Evaluations of cloud properties of global and local cloud system resolving models using CALIPSO and CloudSat simulators. *Journal of Geophysical Research*, **115**, D00H14, doi:10.1029/2009JD012247.

Satoh, M. and Y. Kitao, 2013: Numerical examination of the diurnal variation of summer precipitation over southern China. *SOLA*, **9**, 129–133, doi:10.2151/sola.2013-029.

Satoh, M., T. Matsuno, H. Tomita, H. Miura, T. Nasuno, and S. Iga, 2008: Nonhydrostatic icosahedral atmospheric model (NICAM) for global cloud resolving simulations. *Journal of Computational Physics*, **227 (7)**, 3486–3514, doi:10.1016/j.jcp.2007.02.006.

Satomura, T., 2000: Diurnal variation of precipitation over the Indo-China peninsula: Two-dimensional numerical simulation. *Journal of the Meteorological Society of Japan. Ser. II*, **78 (4)**, 461–475.

Sekiguchi, M. and T. Nakajima, 2008: A k-distribution-based radiation code and its computational optimization for an atmospheric general circulation model. *Journal of Quantitative Spectroscopy and Radiative Transfer*, **109 (17-18)**, 2779–2793, doi:10.1016/j.jqsrt.2008.07.013.

Simpson, J. E., 1994: *Sea breeze and local wind*. First edit ed., Cambridge University Press, Cambridge, United Kingdom, 234 pp.

Skamarock, W., J. Klemp, J. Dudhia, D. Gill, D. Barker, and W. Wang, 2004: A description of the advanced research WRF version 2. Tech. rep., National Center for Atmospheric Research, 88 pp., CO, USA. doi:10.5065/D6DZ069T.

Takane, Y., H. Kusaka, and M. Hara, 2012: Urban climate projection in the 2070's Augusts for the three major metropolitan areas under the IPCC SRES A2 emission scenario: Dynamical downscaling by the WRF-UCM. *Journal of Heat Island Institute International*, **7**, 18–26.

Takata, K., S. Emori, and T. Watanabe, 2003: Development of the minimal advanced treatments of surface interaction and runoff. *Global and Planetary Change*, **38 (1-2)**, 209–222, doi:10.1016/S0921-8181(03)00030-4.

Taniguchi, H., W. Yanase, and M. Satoh, 2010: Ensemble simulation of cyclone nargis by a global cloud-system-resolving model – modulation of cyclogenesis by the Madden-Julian oscillation. *Journal of the Meteorological Society of Japan*, **88 (3)**, 571–591, doi: 10.2151/jmsj.2010-317.

Tomita, H., 2008a: A stretched icosahedral grid by a new grid transformation. *Journal of the Meteorological Society of Japan*, **86A**, 107–119, doi:10.2151/jmsj.86A.107.

Tomita, H., 2008b: New microphysical schemes with five and six categories by diagnostic generation of cloud ice. *Journal of the Meteorological Society of Japan*, **86A**, 121–142, doi:10.2151/jmsj.86A.121.

Tomita, H. and M. Satoh, 2004: A new dynamical framework of nonhydrostatic global model using the icosahedral grid. *Fluid Dynamics Research*, **34 (6)**, 357–400, doi:10.1016/j.fluiddyn.2004.03.003.

Tomita, H., M. Tsugawa, M. Satoh, and K. Goto, 2001: Shallow water model on a modified icosahedral geodesic grid by using spring dynamics. *Journal of Computational Physics*, **174 (2)**, 579–613, doi:10.1006/jcph.2001.6897.

Tompkins, A. M., 2001: Organization of tropical convection in low vertical wind shears: The role of cold pools. *Journal of the Atmospheric Sciences*, **58 (13)**, 1650–1672, doi: 10.1175/1520-0469(2001)058⟨1650:OOTCIL⟩2.0.CO;2.

Warner, T. T., 2010: *Numerical weather and climate prediction*. Cambridge University Press, Cambridge, United Kingdom, 548 pp.

Wilby, R. L., S. P. Charles, E. Zorita, B. Timbal, P. Whetton, and L. O. Mearns, 2004: Guidelines for use of climate scenarios developed from statistical downscaling. Tech. rep., Intergovernmental Panel on Climate Change, 27 pp.

Williams, M. and R. A. Houze, 1987: Satellite-observed characteristics of winter monsoon cloud clusters. *Monthly Weather Review*, **115 (2)**, 505–519, doi:10.1175/1520-0493(1987) 115⟨0505:SOCOWM⟩2.0.CO;2.

Williamson, D. L., J. B. Drake, J. J. Hack, R. Jakob, and P. N. Swarztrauber, 1992: A standard test set for numerical approximations to the shallow water equations in spherical geometry. *Journal of Computational Physics*, **102 (1)**, 211–224, doi:10.1016/S0021-9991(05) 80016-6.

Yamada, Y., K. Oouchi, M. Satoh, H. Tomita, and W. Yanase, 2010: Projection of changes in tropical cyclone activity and cloud height due to greenhouse warming: Global cloud-system-resolving approach. *Geophysical Research Letters*, **37 (7)**, L07 709, doi:10.1029/ 2010GL042518.

Yanase, W., M. Satoh, H. Taniguchi, and H. Fujinami, 2012: Seasonal and intraseasonal modulation of tropical cyclogenesis environment over the bay of Bengal during the extended

summer monsoon. *Journal of Climate*, **25 (8)**, 2914–2930, doi:10.1175/JCLI-D-11-00208.1.

Yasunaga, K., et al., 2006: Changes in the Baiu frontal activity in the future climate simulated by super-high-resolution global and cloud-resolving regional climate models. *Journal of the Meteorological Society of Japan*, **84 (1)**, 199–220, doi:10.2151/jmsj.84.199.

Yatagai, A., P. Xie, and A. Kitoh, 2005: Utilization of a new gauge-based daily precipitation dataset over monsoon Asia for validation of the daily precipitation climatology simulated by the MRI/JMA 20-km-mesh AGCM. *SOLA*, **1**, 193–196, doi:10.2151/sola.2005-050.

Yokoyama, K. and S. Inoue, 2007: Snow cover in Japan under global warming condition. *Gekkan Kaiyo*, **46**, 131–139.